

PARTITIONING OF WATER-SOLUBLE ORGANIC MOLECULES  
AT AEROSOL SURFACE OBSERVED WITH  
SECOND HARMONIC SCATTERING

---

A Dissertation  
Submitted to  
the Temple University Graduate Board

---

In Partial Fulfillment  
of the Requirements for the Degree  
DOCTOR OF PHILOSOPHY

---

by  
Yuhao Wu  
May 2024

Examining Committee Members:

Dr. Hai-Lung Dai, Advisor, Department of Chemistry  
Dr. Francis C. Spano, Committee Chair, Department of Chemistry  
Dr. Daniel R. Strongin, Department of Chemistry  
Dr. Chen Wang, External Member, Department of Chemistry and Biochemistry,  
Queens College, City University of New York

©  
Copyright  
2024

by

Yuhao Wu  
All Rights Reserved

## ABSTRACT

Aerosol particles are important in air quality, climate, and human health. They can affect the earth's energy budget directly by scattering and absorbing solar radiation and serve as cloud condensation nuclei (CCN), thus influencing cloud properties and lifetime. Atmospheric aerosols are formed through a wide variety of natural and anthropogenic sources.

This dissertation presents a comprehensive investigation into the behavior of water-soluble organic molecules on atmospheric aerosol surfaces using Second Harmonic Scattering (SHS). The study focuses on understanding the partitioning of these molecules at the aerosol surface, a crucial aspect in atmospheric chemistry impacting cloud formation, radiation balance, and air quality.

The research is divided into three main parts. Initially, the study explores the disposition of organic molecules on aerosol surfaces, utilizing a modified Langmuir model to describe their behavior. This part emphasizes the predominant residence of these molecules on the aerosol surface, highlighting the surface's significant role in atmospheric reactions.

The second part examines the interactions between salts and organic molecules on the aerosol surface. A series of experiments with varying salts reveal how different ions influence the partitioning behavior of organic molecules, underscoring the importance of ionic species in governing aerosol surface dynamics.

The final part of the study reveals a significant difference between the aerosol and planar air-water interfaces. The equilibrium rate constant for aerosols is found to be tenfold faster, indicating a larger Gibbs free energy, contrasting with the planar air-water interface scenario. And aerosol surfaces exhibit lower molecular density due to the finite availability of organic molecules. These findings highlight aerosol surfaces' unique kinetic and thermodynamic behaviors compared to their planar counterparts.

This work significantly advances our understanding of aerosols, their surfaces, and the various factors influencing their behavior in the atmosphere. The findings have crucial implications for our comprehension of climate change, air quality, and aerosols' environmental and health impacts. The introduction of a novel in-situ technique for detecting organic molecules at aerosol surfaces marks a breakthrough in aerosol research, offering insights into the distribution and interactions of these molecules within atmospheric particles.

To my loving parents, Xiuli Wu and Huazhi Wang, who have always believed in me and supported my academic pursuits. Your unwavering faith and encouragement have been my guiding lights in this journey.

And to my mentor, Professor Hai-Lung Dai, whose insights and guidance have been invaluable in shaping my research and academic growth. Thank you for your patience, wisdom, and belief in my potential.

## ACKNOWLEDGMENTS

I would like to take this opportunity to extend my sincere thanks to everyone who has helped make this thesis possible and better.

My deepest gratitude goes first and foremost to my advisor, Professor Hai-Lung Dai. He has been a tremendous mentor to me. I am immensely thankful for his great support and encouragement during my time at Temple University. His advice on both my research and future career has been invaluable.

I would also like to express my appreciation to my committee members, Professor Strongin, Professor Spano, and Professor Wang, for their invaluable time, insightful comments, and encouragement towards my research.

A special thanks goes to my parents. Although I have not met them in person for over five years, their spiritual support has always encouraged me to overcome difficulties. The values they instilled in me have helped me grow and become who I am today. I can never repay the love and support they have given me.

I am also grateful to Dr. Yi Rao, Dr. Jianxin Chen, Dr. Jianqiang Ma, and Dr. Michael J. Wilhelm for their generous help with my research. My gratitude extends to other former and current members of the Dai Group: Dr. Xiaohua Hu, Dr. Grace Purnell, Dr. Tong Wu, Yujie Li, Julianne Mason, Dr. Bolei Xu, Yajing Wu, Dr. Jonathan Smith, Dr. Jun Han, Dr. Mohammad Sharifin Gh., Dr. Hui Fang, Dr. Lei Jin, Dr. Chao He, and Huatao Yin, for their assistance and camaraderie.

# TABLE OF CONTENTS

	Page
ABSTRACT.....	iii
DEDICATION.....	v
ACKNOWLEDGMENTS .....	vi
LIST OF TABLES.....	ix
LIST OF FIGURES .....	x
CHAPTER	
1. INTRODUCTION .....	1
1.1 Aerosols .....	1
1.2 Aerosol Air-water Interface .....	3
1.3 Analytical Techniques .....	6
1.4 Second Order Non-linear Optics.....	7
1.5 Theory of Second Harmonic Generation .....	9
1.6 Aim and Scope of this Dissertation .....	13
1.7 Bibliography .....	14
2. ELUCIDATING THE PARTITIONING BEHAVIOR OF WATER- SOLUBLE ORGANIC MOLECULES ON AEROSOL SURFACES: A SECOND HARMONIC SCATTERING APPROACH .....	19
2.1 Introduction.....	19
2.2 Experiment.....	21
2.2.a Aerosol Generation .....	21

2.2.b SHS Setup .....	23
2.2.c Material .....	23
2.2.d Aerosol Characterization .....	26
2.3 Fitting Model .....	28
2.4 Result and Discussion .....	30
2.5 Conclusion .....	37
2.6 Bibliography .....	39
3. SALT IMPACT ON PARTITIONING DYNAMICS OF WATER-SOLUBLE ORGANIC MOLECULES IN AEROSOL SURFACE CHEMISTRY .....	41
3.1 Introduction.....	41
3.2 Experiment.....	43
3.3 Result and Discussion.....	44
3.4 Conclusion .....	49
3.5 Bibliography .....	51
4. COMPARATIVE ANALYSIS OF CURVED AEROSOL AND PLANAR AIR-WATER INTERFACES.....	53
4.1 Introduction.....	53
4.2 Experiment.....	54
4.3 Result and Discussion.....	55
4.4 Conclusion .....	62
4.5 Bibliography .....	63
5. CONCLUSION AND PROSPECTIVES .....	65

## LIST OF TABLES

Table	Page
1. DiA-4 maximum number density at the aerosol surface $N_{\max}$ , equilibrium constant $k$ , and Gibbs free energy $\Delta G$ of NaCl aerosols and $(\text{NH}_4)_2\text{SO}_4$ aerosols.....	35
2. Langmuir model fitting parameters of aerosols with different salts .....	49
3. Rate constant $k$ of aerosol and flat air-water interface with corresponding Gibbs free energy $\Delta G$ .....	58

## LIST OF FIGURES

Figure	Page
1. (A) Geometry of second-harmonic generation, and (B) energy-level diagram of second-harmonic generation.....	12
2. Schematics of laboratory aerosol generator (Model 3076 left) and the atomizer assembly block (right) .....	24
3. A schematic of second harmonic scattering experimental setup of laboratory generated aerosols .....	25
4. The chemical structure of DiA-4 and corresponding UV-Vis spectrum .....	25
5. (a) Particle size measured by scanning mobility particle sizer (SMPS) and (b) corresponding SHS intensity as a function of particle diameter.....	27
6. Spectra of second harmonic scattered signal from DiA-4-containing model NaCl aerosols.....	32
7. Langmuir isotherm of SHS signal of (a) NaCl aerosols and (b) (NH <sub>4</sub> ) <sub>2</sub> SO <sub>4</sub> aerosols, respectively.....	33
8. DiA-4 partition at aerosol surface of (a) 100nm radius aerosols and (b) 2.5μm diameter aerosols (PM 2.5).....	38
9. Langmuir isotherm of SHS signal and corresponding fitting curve of a) (NH <sub>4</sub> ) <sub>2</sub> SO <sub>4</sub> aerosols, b) NH <sub>4</sub> Cl aerosols, and c) NH <sub>4</sub> NO <sub>3</sub> , respectively.....	46
10. MD simulation results of air-water interface with different salts from Dr. Tobias publications. Left: snapshot from MD results. Right: density profiles of salt ions and water oxygens from the center of the slab (z = 0) to the air/ water interface.....	50
11. A schematic of second harmonic generation experimental setup for planar surface.....	55
12. Comparison of SHS signal of 1M NaCl aerosols (grey) and SHG signals of 1M NaCl solution air-water interface.....	56
13. Depiction of the equilibrium between bulk and surface in (a) aerosol and (b) flat air-water interface.....	61

# CHAPTER 1 INTRODUCTION

## 1.1 Aerosols

Atmospheric particulate matter (PM), also known as atmospheric aerosols, encompasses many liquid and solid particles suspended in the Earth's atmosphere. These particles exhibit complex chemical compositions, incorporating high concentrations of inorganic salt, myriad organic molecules, and a size range spanning from a few nanometers to tens of micrometers. (1)

Particles on the larger end of the spectrum, akin in size to fine drizzle or sand, often rapidly settle out of the atmosphere due to their substantial size, thus having minimal impact on atmospheric chemistry. In contrast, particles ranging from 0.002- to 10-  $\mu\text{m}$  are vital to atmospheric chemistry and physics due to their longevity in the atmosphere.(2)

In classification terms, aerosol particles with diameters no larger than 2.5  $\mu\text{m}$  are called "fine particles" or PM 2.5. "Coarse particles," on the other hand, measure between 2.5 to 10 micrometers in diameter.(3) Their minuscule size is remarkable, significantly smaller than human hair, which averages tens of microns in width. While aerosols are usually defined by radius, not all atmospheric particles maintain a perfect spherical shape. Thus, for irregularly shaped particles, the concept of geometrical radii loses relevance, and an "effective radius," based on its physical properties, is used instead.

Atmospheric aerosols are generally classified into two categories: primary and secondary aerosols. Primary aerosols are emitted directly into the atmosphere and originate from various sources. These include combustion processes (such as fossil fuel burning for transportation and energy production, biomass burning from deforestation and agricultural waste, and domestic cooking fires), volcanic eruptions, and other natural sources like bacteria, fungal spores, and plant debris. Wind-driven processes, such as dust resuspension and sea spray, also contribute to aerosol production.(4,5) Secondary aerosols, on the other hand, result from complex atmospheric photochemical reactions involving primary aerosols, which react with atmospheric oxidants or undergo UV light irradiation.(6,7) This process generates new, less volatile species on the aerosol surface or within the particle.

Consider sea spray aerosol, which is produced when ocean surface bubbles burst or waves crest when wind speeds exceed 7-11 m/s. These particles comprise a complex system laden with sea salt and organic components, including lipids and bacteria.(8) Although sea spray particles are classified as primary aerosols, they can serve as catalysts for photochemical reactions, thus forming secondary aerosols. With their intricate composition, aerosol particles are influenced by various factors such as geographical location, temporal variations, temperature, relative humidity, and regional primary aerosol sources. This leads to aerosols with unique composition signatures, like marine aerosols abundant with  $\text{Na}^+$  and  $\text{Cl}^-$  or forest aerosols containing more  $\text{NH}_4^+$  and  $\text{NO}_x$ .(5,9)

Atmospheric aerosols are pivotal in air quality, climate, and human health. They directly impact the Earth's energy balance by scattering and absorbing solar radiation. For instance, by scattering light, aerosol particles can reduce visibility and generate negative radiative forcing, leading to atmospheric cooling. Conversely, the absorption of light by aerosols contributes to positive radiative forcing, causing atmospheric warming.<sup>(10)</sup> Moreover, these particles can serve as cloud condensation nuclei (CCN), influencing the characteristics of clouds, such as their size distribution, quantity, and lifespan.<sup>(6)</sup> Importantly, aerosols can also facilitate the transmission of biological organisms and pathogens, potentially leading to respiratory diseases and allergies.<sup>(11)</sup>

Sea spray aerosols are particularly significant among all atmospheric aerosol particles due to their immense global emissions of primary organic matter, amounting to  $\sim 9$  Tg/yr in the sub-micron size range, compared to a total global annual emission of primary organics of 75 Tg/yr.<sup>(8,12)</sup> These particles' influence is especially noteworthy considering that oceans cover approximately  $\sim 70\%$  of the Earth's surface, and the wind can easily disperse these fine particles over large areas. As research progresses, our understanding of the role and impact of aerosols in areas like cloud formation, weather patterns, and even climate change will likely expand, underlining the need for continuous monitoring and investigation of these crucial atmospheric constituents.

## **1.2 Aerosol air-water interface**

Atmospheric aerosols constitute a substantial fraction of small particle mass globally and are an amalgamation of complex physical and chemical processes. With

secondary organic aerosols (SOA) forming a major part, these processes include adsorption of volatile organic compounds (VOCs) and semi-volatile organic compounds (SVOCs) to the aerosol surface, transfer of organic molecules from bulk to the surface, and various surface reactions.*(13–15)*

Aerosol surfaces play a critical role in these transformations, facilitating chemical exchanges between the aerosol and gas phases as well as serving as reaction sites for photochemical reactions. Surrounded by potent oxidants like ozone, •OH, and NO<sub>x</sub> in the atmosphere, adsorbed organic molecules can readily undergo oxidation reactions, generating new species that can impact the properties of the aerosol particles and, in turn, significantly influence the environment.*(6)* As an example interfacial reactions between ozone and sodium bromide aerosol particles, leading to the production of Br<sub>2</sub>, with the reaction rate often competing with or exceeding bulk aqueous reactions.*(16)*

Furthermore, aerosol surfaces interact with other atmospheric constituents, such as sulfur dioxide (SO<sub>2</sub>) and ammonia (NH<sub>3</sub>), forming secondary inorganic aerosols like sulfates and nitrates. These species are significant contributors to visibility degradation and atmospheric acidification.*(17)*

While it's common to model aerosol interfaces as planar air-water interfaces, the reality is far more complex due to their three-dimensional nature. Aerosol particles, due to their smaller size and higher curvature, exhibit different characteristics, such as a higher surface-to-volume ratio and altered surface tension, which can significantly

influence the rate and extent of gas-particle interactions. Their unique curvature could also impact the orientation and packing of surface-adsorbed molecules, thereby influencing the rate of surface reactions.(18)

Considering aerosols as air-water interfaces also underscores the role of environmental factors in modulating their behavior. For instance, solar radiation intensity and wavelength, atmospheric humidity, temperature, as well as the presence of catalytic surfaces like mineral dust or black carbon, influence the photochemical reactions on aerosol surfaces. Black carbon, primarily emitted from anthropogenic combustion processes, offers a unique catalytic surface that enhances certain atmospheric chemical reactions.(19,20)

Moreover, aerosols carry biogeochemical implications, serving as key vectors for the global distribution of nutrients like iron and phosphorus to nutrient-limited ecosystems, including vast expanses of the ocean. This links aerosol dynamics directly to Earth's carbon cycle, enhancing primary productivity in these regions.

This layered complexity of aerosols necessitates an interdisciplinary approach for a comprehensive understanding, encompassing the realms of atmospheric chemistry, physics, biology, and climate science. Considering these multifaceted interactions and impacts, the urgent need for *in-situ* aerosol characterization techniques and further refinement in climate models becomes clear.

### 1.3 Analytical techniques

Over the years, various analytical techniques have been developed to investigate the complex chemical composition of aerosol particles. Traditional methods primarily rely on off-line measurements, including gas chromatography/mass spectrometry (GC/MS), liquid chromatography/mass spectrometry (LC/MS), nuclear magnetic resonance (NMR),(21) and Fourier transform infrared (FTIR) spectroscopy.(22) These techniques, while effective, present a significant limitation - they do not distinguish between the surface and bulk composition of aerosol particles.

For instance, GC/MS, renowned for its high separation resolution and identification capability, has been extensively used to analyze a broad spectrum of water-soluble organic compounds (WSOCs).(4) Similarly, NMR provides valuable information about the molecular structure and quantification of the samples. Additionally, the morphology of aerosol particles has been studied in detail using electron microscopy (EM).(23)

However, these off-line methodologies involve the pre-collection of aerosol samples, which are then subjected to analysis. This step could potentially induce changes in the chemical composition and morphology of the particles during the collection and transportation process, leading to results that may not accurately reflect the aerosols' original state in the atmosphere.

Recognizing these limitations, the scientific community has called for developing *in-situ* or online measurement techniques for aerosols. Advances in this field have led to the creation of methods such as cryo-transmission electron microscopy (cryo-TEM), which can rapidly capture the hydrated structure of aerosol particles, preserving their nascent state.<sup>(8)</sup> Moreover, instruments like the Condensation Particle Counter (CPC) and Differential Mobility Analyzer (DMA) offer real-time particle number density and size measurements. These innovations, coupled with online aerosol mass spectrometry tools such as Aerosol Time of Flight Mass Spectrometer (ATOFMS) and Aerosol Mass Spectrometer, have significantly expanded our ability to study aerosol particles.<sup>(24)</sup>

Nonetheless, a pressing need remains for an online measurement technique capable of distinguishing between aerosol particles' surface and bulk components. In this thesis, I introduce a groundbreaking technique for the *in-situ* detection of organic molecules at aerosol surfaces. A defining feature of our approach is its unique capability to discern the partitioning of WSOCs between the aerosol surface and bulk. This innovation fills a critical gap in aerosol research, offering unprecedented insights into the distribution and interactions of WSOCs within aerosol particles, which can deepen our understanding of these vital atmospheric constituents' environmental and health impacts.

#### **1.4 Second order nonlinear optics**

Second Harmonic Generation (SHG) and Second Harmonic Scattering (SHS) stand out as particularly effective techniques in the family of nonlinear optical methods for investigating the properties of interfaces. These methods have evolved from their

foundational discovery in the 1960s to now providing researchers with an extraordinary lens for studying complex physical and chemical phenomena at interfaces.(25–28)

SHG is a second-order nonlinear process whereby two photons interact with a nonlinear material, denoted as  $\chi(2)$ , under an intense light source at frequency  $\omega$ . This interaction generates a new photon at twice the frequency,  $2\omega$ , effectively halving the wavelength of the original photons. This fascinating process was first observed in 1961 by Franken et al. when intense light from a ruby optical maser was shone onto a noncentrosymmetric crystalline quartz crystal, resulting in SHG at a different wavelength. The findings spurred a significant number of theoretical studies and applications in various media, including crystals, metal surfaces, and the air-water interface.

The surface sensitivity of SHG makes it an indispensable tool across various research fields. Pioneering work by Shen and others has transformed SHG into a versatile tool for exploring different interfaces, as well as buried interfaces. From studying many dye molecules, surfactants, and proteins to examining micro-sized particles dispersed in liquid, SHG continues to be a powerful approach in the scientific exploration of interfaces.(29,30)

A related phenomenon, Hyper Rayleigh Scattering (HRS), also occurs when light scattered at twice the frequency. Despite the similarity, HRS differs as a spontaneous and incoherent process that originates from local density or orientation fluctuations.(31)

In the context of aerosol research, our group, in collaboration with others, has extended SHG to the surface of nano-sized colloidal particles. This work has opened up new avenues for studying sub-micron-sized aerosol particles and their surfaces. This thesis will showcase and discuss the results of these novel SHG and SHS applications on aerosol particles.<sup>(26,32)</sup>

An even more exciting development is Second Harmonic Scattering (SHS), a variant of SHG, which allows the exploration of non-planar or microscopic interfaces such as those found in aerosols. Unlike SHG, the SHS signal is scattered in all directions, allowing for examining complex microscopic particles in suspension, such as aerosols. Through SHS, we can probe the properties of individual particles, providing insights into their size, shape, and composition of the surface and interface in real-time.

The fusion of these analytical techniques presents a significant advancement in aerosol research, especially with the unique capability to distinguish the partitioning of water-soluble organic compounds between the aerosol surface and bulk.

## **1.5 Theory of Second Harmonic Generation**

Second Harmonic Generation (SHG) is a non-linear optical process where photons with a frequency  $\omega$  interact with a nonlinear medium ( $\chi^{(2)}$ ), leading to the creation of a photon at twice the frequency, or  $2\omega$ , as illustrated in Figure 1.1. This process was first documented by Franken and colleagues in 1961, just after the development of the first optical laser. They detected SHG at  $3472\text{\AA}$  in a specific type of

quartz crystal when it was illuminated by a ruby optical maser that emitted a pulse of 6943Å light within a millisecond. This pioneering discovery led to additional studies in 1962 that used Maxwell's equations to delve deeper into the behavior of SHG in certain materials.

The simple yet powerful nature of SHG has generated significant interest over the years. Its application spans various materials, from crystals and metals to the air-water boundary. Thanks to groundbreaking work by Shen and others, SHG has evolved into a crucial tool for studying various interfaces, even those that aren't immediately visible.

Alongside SHG, there's another interesting phenomenon called Hyper Rayleigh Scattering (HRS). In HRS, the focus is on measuring the intensity of scattered light at the frequency  $2\omega$ . Unlike SHG, HRS is a more random and dispersed process resulting from slight changes in density or orientation.

In the realm of SHG research, various compounds like dyes, surfactants, and proteins have been closely examined. The Eisenthal group, for instance, identified SHG signals from tiny particles suspended in liquid. Building on these findings, our team, in collaboration with other researchers, has expanded this exploration to the surfaces of even smaller nanoscale particles. This thesis will present our findings on SHG signals from these minuscule aerosol particles.(33)

This process is described by the equation  $P_S^{(2)}(\omega) = \chi_S^{(2)} E'(\omega) E'(\omega)$ , where  $P_S^{(2)}(\omega)$  is the second-order nonlinear surface polarization,  $\chi_S^{(2)}$  is the second-order surface susceptibility tensor and  $E'(\omega)$  is the driving field at the fundamental frequency. SHG is particularly sensitive to surface and interface properties due to the nature of the nonlinear susceptibility tensor.

In the context of colloidal systems, the theoretical frameworks of Nonlinear Rayleigh-Gans-Debye (NLRGD) and Nonlinear Mie (NLM) theories are often employed to describe the SH scattered light from colloidal particles.<sup>(34)</sup> These theories account for factors like particle size, shape, and composition, which can significantly affect the SHG phenomenon.

A critical aspect of SHG studies is relating the molecular hyperpolarizability ( $\beta$ ) of molecules to the second-order surface susceptibility ( $\chi^{(2)}$ ). The SH intensity is also proportional to the square of the coverage of SH-active molecules on the surface, which can be mathematically expressed and related to the surface molecular density ( $N_S$ ). The relationship between the molecular density of adsorbed molecules ( $N_S$ ) and the molecular concentration in the bulk solution ( $C$ ) is often described using the Langmuir adsorption model.

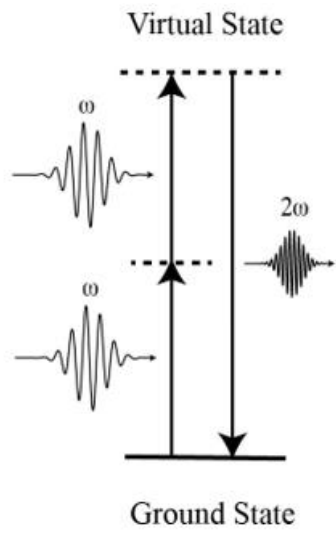
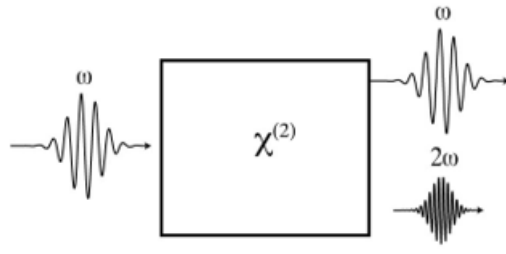


**Figure 1.1** (A) Geometry of Second Harmonic Generation, and (B) Energy diagram of the Second Harmonic Generation

## **1.6 Aim and scope of this dissertation.**

In this dissertation, I present a groundbreaking exploration into the behavior of water-soluble organic molecules on atmospheric aerosol surfaces using Second Harmonic Scattering (SHS). This research is segmented into three main components, each significantly enhancing our understanding of aerosol behavior and their critical role in atmospheric chemistry and processes, particularly affecting cloud formation, radiation balance, and air quality.

The initial segment of our study offers novel insights into the disposition of organic molecules on aerosol surfaces. Our findings indicate a predominant residency of these molecules at the aerosol surface, highlighting the surface's vital role in atmospheric reactions. To better describe this observed behavior, we have advanced the traditional Langmuir model, refining it to portray the real-world scenario in aerosols more accurately. Our modified model accounts for the finite availability of organic molecules within the aerosol bulk, a crucial factor in understanding their surface interactions.

In the second portion of the research, we focus on the interactions between salts and organic molecules at the aerosol surface. A series of experiments with various salts demonstrate how different ionic species significantly influence the partitioning behavior of organic molecules. This part of the work underscores the importance of ion-specific effects in governing the dynamics at the aerosol air-water interface.

The final part of the dissertation contrasts the behavior at the aerosol air-water interface with that at the planar air-water interface. Our studies reveal significant differences between these two scenarios in the rate constants and Gibbs free energy. While the aerosol surface exhibits a rate constant tenfold faster and a larger Gibbs free energy, the planar air-water interface shows a lower surface molecular density due to the finite availability of organic molecules in aerosols (~10 molecules/particle). In contrast, with its virtually infinite bulk supply, the planar liquid surface shows a significantly higher molecular density.

Through these interconnected research areas, this dissertation significantly extends our understanding of aerosols, their surfaces, and the numerous factors influencing their behavior in the atmospheric context. The insights gained are vital for our comprehension of climate change, air quality, and the broader environmental and health impacts of aerosols.

## 1.7 Bibliography

1. Bluhm, H.; Siegmann, H. C. Surface science with aerosols. *Surface Science* **2009**, *603*(10–12), 1969–1978. doi:10.1016/j.susc.2008.08.041.
2. Blanchard, D. C. The ejection of drops from the sea and their enrichment with bacteria and other materials: A review. *Estuaries* **1989**, *12*(3), 127–137. doi:10.2307/1351816.
3. Jahedi, F.; Dehdari Rad, H.; Goudarzi, G.; Tahmasebi Birgani, Y.; Babaei, A. A.; Ahmadi Angali, K. Polycyclic aromatic hydrocarbons in PM1, PM2.5 and PM10 atmospheric particles: identification, sources, temporal and spatial variations. *Journal of Environmental Health Science and Engineering* **2021**, *19*(1), 851–866. doi:10.1007/s40201-021-00652-7.

4. Graham, B.; Mayol-Bracero, O. L.; Guyon, P.; Roberts, G. C.; Decesari, S.; Facchini, M. C.; et al. Water-soluble organic compounds in biomass burning aerosols over Amazonia I. Characterization by NMR and GC-MS. *Journal of Geophysical Research Atmospheres* **2002**, *107*(20), LBA 14-1-LBA 14-16. doi:10.1029/2001JD000336.
5. Kolb, C. E.; Worsnop, D. R. Chemistry and Composition of Atmospheric Aerosol Particles. *Annual Review of Physical Chemistry* **2012**, *63*(1), 471–491. doi:10.1146/annurev-physchem-032511-143706.
6. Novak, G. A.; Bertram, T. H. Reactive VOC Production from Photochemical and Heterogeneous Reactions Occurring at the Air-Ocean Interface. *Accounts of Chemical Research* **2020**, *53*(5), 1014–1023. doi:10.1021/acs.accounts.0c00095.
7. Tsui, W. G.; Rao, Y.; Dai, H. L.; McNeill, V. F. Modeling Photosensitized Secondary Organic Aerosol Formation in Laboratory and Ambient Aerosols. *Environmental Science and Technology* **2017**, *51*(13), 7496–7501. doi:10.1021/acs.est.7b01416.
8. Patterson, J. P.; Collins, D. B.; Michaud, J. M.; Axson, J. L.; Sultana, C. M.; Moser, T.; et al. Sea spray aerosol structure and composition using cryogenic transmission electron microscopy. *ACS Central Science* **2016**, *2*(1), 40–47. doi:10.1021/acscentsci.5b00344.
9. Jimenez, J. L.; Canagaratna, M. R.; Donahue, N. M.; Prevot, A. S. H.; Zhang, Q.; Kroll, J. H.; et al. Evolution of organic aerosols in the atmosphere. *Science* **2009**, *326*(5959), 1525–1529. doi:10.1126/science.1180353.
10. Valsaraj, K. T. A Review of the Aqueous Aerosol Surface Chemistry in the Atmospheric Context. *Open Journal of Physical Chemistry* **2012**, *02*(01), 58–66. doi:10.4236/ojpc.2012.21008.
11. Li, J.; Leavey, A.; Wang, Y.; O’Neil, C.; Wallace, M. A.; Burnham, C. A. D.; et al. Comparing the performance of 3 bioaerosol samplers for influenza virus. *Journal of Aerosol Science* **2018**, *115*(August 2017), 133–145. doi:10.1016/j.jaerosci.2017.08.007.
12. T. Cravigan, L.; D. Mallet, M.; Vaattovaara, P.; J. Harvey, M.; S. Law, C.; L. Modini, R.; et al. Sea spray aerosol organic enrichment, water uptake and surface tension effects. *Atmospheric Chemistry and Physics* **2020**, *20*(13), 7955–7977. doi:10.5194/acp-20-7955-2020.

13. Brauer, C. S.; Blake, T. A.; Guenther, A. B.; Sharpe, S. W.; Sams, R. L.; Johnson, T. J. Quantitative infrared absorption cross sections of isoprene for atmospheric measurements. *Atmospheric Measurement Techniques* **2014**, *7*(11), 3839–3847. doi:10.5194/amt-7-3839-2014.
14. Bao, H.; Niggemann, J.; Luo, L.; Dittmar, T.; Kao, S. J. Molecular composition and origin of water-soluble organic matter in marine aerosols in the Pacific off China. *Atmospheric Environment* **2018**, *191*(December 2017), 27–35. doi:10.1016/j.atmosenv.2018.07.059.
15. Simon, V.; Luchetta, L.; Torres, L. Estimating the emission of volatile organic compounds (VOC) from the French forest ecosystem. *Atmospheric Environment* **2001**, *35*(SUPPL. 1). doi:10.1016/s1352-2310(00)00565-3.
16. Fan, S.; Jacob, D. J. Surface ozone depletion in Arctic spring sustained by bromine reactions on aerosols. *Nature* **1992**, *359*(October), 522–524.
17. Wang, C.; Lei, Y. D.; Wania, F. Effect of sodium sulfate, ammonium chloride, ammonium nitrate, and salt mixtures on aqueous phase partitioning of organic compounds. *Environmental Science and Technology* **2016**, *50*(23), 12742–12749. doi:10.1021/acs.est.6b03525.
18. Ahn, W. S.; Jhon, M. S.; Pak, H.; Chang, S. Surface tension of curved surfaces. *Journal of Colloid And Interface Science* **1972**, *38*(3), 605–608. doi:10.1016/0021-9797(72)90395-5.
19. Zhao, G.; Tan, T.; Zhu, Y.; Hu, M.; Zhao, C. Method to quantify black carbon aerosol light absorption enhancement with a mixing state index. *Atmospheric Chemistry and Physics* **2021**, *21*(23), 18055–18063. doi:10.5194/acp-21-18055-2021.
20. Bond, T. C.; Doherty, S. J.; Fahey, D. W.; Forster, P. M.; Berntsen, T.; Deangelo, B. J.; et al. Bounding the role of black carbon in the climate system: A scientific assessment. *Journal of Geophysical Research Atmospheres* **2013**, *118*(11), 5380–5552. doi:10.1002/jgrd.50171.
21. Mohimani, H.; Gurevich, A.; Mikheenko, A.; Garg, N.; Nothias, L.-F.; Ninomiya, A.; et al. Characterization of water-soluble organic matter in urban aerosol by 1 H-NMR spectroscopy. *Physiology & behavior* **2017**, *176*(3), 139–148. doi:10.1016/j.atmosenv.2015.12.067.Characterization.

22. Nájera, J. J.; Horn, A. B. Infrared spectroscopic study of the effect of oleic acid on the deliquescence behaviour of ammonium sulfate aerosol particles. *Physical Chemistry Chemical Physics* **2009**, *11*(3), 483–494. doi:10.1039/b812182f.
23. Brostrøm, A.; Kling, K. I.; Hougaard, K. S.; Mølhav, K. Complex Aerosol Characterization by Scanning Electron Microscopy Coupled with Energy Dispersive X-ray Spectroscopy. *Scientific Reports* **2020**, *10*(1), 1–15. doi:10.1038/s41598-020-65383-5.
24. Wilson, J. M.; Baeza-Romero, M. T.; Jones, J. M.; Pourkashanian, M.; Williams, A.; Lea-Langton, A. R.; et al. Soot formation from the combustion of biomass pyrolysis products and a hydrocarbon fuel, n-decane: An aerosol time of flight mass spectrometer (ATOFMS) study. *Energy and Fuels* **2013**, *27*(3), 1668–1678. doi:10.1021/ef3019386.
25. Zhuang, X.; Miranda, P. B.; Kim, D.; Shen, Y. R. Mapping molecular orientation and conformation at interfaces by surface nonlinear optics. *Physical Review B - Condensed Matter and Materials Physics* **1999**, *59*(19), 12632–12640. doi:10.1103/PhysRevB.59.12632.
26. Wang, H.; Troxler, T.; Yeh, A. G.; Dai, H. L. In situ, nonlinear optical probe of surfactant adsorption on the surface of microparticles in colloids. *Langmuir* **2000**, *16*(6), 2475–2481. doi:10.1021/la9909087.
27. Shen, Y. Optical Second Harmonic Generation At Interfaces. *Annual Review of Physical Chemistry* **1989**, *40*(1), 327–350. doi:10.1146/annurev.physchem.40.1.327.
28. Shen, Y. R. Surface properties probed by second-harmonic and sum-frequency generation. *Nature*. 1989, pp 519–525. doi:10.1038/337519a0.
29. Blanchard-Desce, M. H.; Ventelon, L.; Charier, S.; Moreaux, L.; Mertz, J. Molecular probes for nonlinear optical imaging of biological membranes. *Linear and Nonlinear Optics of Organic Materials* **2001**, *4461*(December 2001), 20. doi:10.1117/12.449848.
30. Xu, Z.; Dong, Y. Probing the dielectric property of organic molecules at solid-liquid interfaces using reflection second harmonic generation. *Surface Science* **2000**, *445*(2–3). doi:10.1016/S0039-6028(99)01132-2.
31. Das, P. K. Chemical applications of hyper-rayleigh scattering in solution. *Journal of Physical Chemistry B* **2006**, *110*(15), 7621–7630. doi:10.1021/jp0562983.

32. Wang, H.; Yan, E. C. Y.; Liu, Y.; Eisenthal, K. B. Energetics and population of molecules at microscopic liquid and solid surfaces. *Journal of Physical Chemistry B* **1998**, *102*(23), 4446–4450. doi:10.1021/jp980491y.
33. Wu, Y.; Li, W.; Xu, B.; Li, X.; Wang, H.; McNeill, V. F.; et al. Observation of Organic Molecules at the Aerosol Surface. *Journal of Physical Chemistry Letters* **2016**, *7*(12), 2294–2297. doi:10.1021/acs.jpcllett.6b00872.
34. Gonella, G.; Dai, H. L. Second harmonic light scattering from the surface of colloidal objects: Theory and applications. *Langmuir* **2014**, *30*(10), 2588–2599. doi:10.1021/la403570f.

# **CHAPTER 2 ELUCIDATING THE PARTITIONING BEHAVIOR OF WATER-SOLUBLE ORGANIC MOLECULES ON AEROSOL SURFACES: A SECOND HARMONIC SCATTERING APPROACH**

## **2.1 Introduction**

Atmospheric aerosols, comprised of solid particles or liquid droplets suspended in air and containing inorganic salts and organic molecules, play a crucial role in the Earth's climate system. They contribute to air pollution, impact air quality, radiation balance, and cloud formation through the process of scattering solar radiation and participating in the hydrological cycle. Marine aerosols, originating from the ocean, and urban aerosols, resulting from anthropogenic activities such as traffic and industrial emissions, possess distinct sources and chemical compositions, influencing their interactions with the environment.<sup>(1,2)</sup>

Water-soluble organic molecules are a vital component of atmospheric aerosols. Their partitioning at the aerosol surface can impact the aerosol's physical and chemical properties, including hygroscopicity, optical and cloud-nucleating properties, reactivity, and secondary organic aerosol formation.<sup>(3,4)</sup> Researchers analyzed aerosols' composition and mass fraction of organic molecules. However, isolating the organic molecules at the aerosol surface from the bulk is challenging. Despite their importance, the partitioning behavior of water-soluble organic molecules at the aerosol surface still

needs to be fully understood, particularly under various environmental conditions, such as the presence of inorganic salts.

Traditional analytical techniques, including UV-VIS spectroscopy, IR spectroscopy, Raman spectroscopy, NMR, and GC-MS, have been used to analyze the composition of environmental airborne aerosols.<sup>(5–7)</sup> However, these techniques have limitations when studying the partitioning of molecules on the aerosol surface. Second Harmonic Scattering (SHS), a surface-sensitive nonlinear optical technique based on Second Harmonic Generation (SHG), offers a powerful tool for studying molecules at the aerosol surface at the sub-nanometer scale. SHS has been utilized to quantitatively characterize various surfaces of colloidal particles, liposome membranes, and biological cells. The intrinsic sensitivity of SHG to surfaces/interfaces of matters with inversion symmetry allows for the selective detection of molecules localized at the aerosol surface. Molecules in the interior bulk of aerosols are randomly oriented, yielding no coherent SHG signal. In contrast, the center of inversion symmetry is broken at the air-aerosol interface, enabling molecules at the aerosol surface to generate an SHS signal, which scales quadratically with the molecular surface density.<sup>(8,9)</sup>

In a prior proof-of-principle study, our laboratory used SHS to detect the hemicyanine dye, trans-4-[4-(dibutylamino)styryl]-1-methylpyridinium iodide (DiA-4), at the surface of laboratory made sea-salt aerosols.<sup>(10)</sup> Like organic compounds commonly found in atmospheric aerosols (e.g., fatty acids, terpenes, etc.), DiA-4 is amphiphilic and contains both hydrophobic and hydrophilic functionality.<sup>(11)</sup> DiA-4

exhibits an optical absorption near 475 nm, facilitating a resonantly enhanced SHS response.

In this chapter, we used SHS to examine the partition of surfactant dye molecules in lab-generated Sodium Chloride (NaCl) and Ammonium Sulfate ((NH<sub>4</sub>)<sub>2</sub>SO<sub>4</sub>) aerosols to represent the sea-salt and urban aerosols, respectively. We use the hemicyanine dye, DiA-4, as a representative water-soluble organic molecule. We investigate the concentration-dependent surface coverage of DiA-4 in both aerosol types and analyze the data with Langmuir fitting model. We further calculated the partitioning of water-soluble organic molecules at the aerosol surface. Results revealed that over 90% of the organic molecules are at the aerosol surface when their concentrations are lower than 1 μM. In other words, almost all the trace water-soluble organic molecules in the aerosols stay on the aerosol surface. We need to consider aerosol surface properties when learning aerosol reactions.

## **2.2 Experiment**

### ***2.2.a Aerosol Generation***

Aerosols were prepared using a commercial aerosol generator (TSI Co. Model 3076). A scanning mobility particle sizer (SMPS, TSI 3938L87) was used to measure the size distribution of the aerosols and particle number densities. The average diameter of aerosols generated from 1M NaCl solution was ~100 nm, and the typical number densities were 10<sup>7</sup> particles per cm<sup>3</sup>. Aerosols are carried by a nitrogen flow with a

pressure of around 30 psi. Once prepared, the ensemble of aerosols traveled ~ 1 m through a plastic tube before arriving at the focal point of the fundamental laser light used for the SHS. There are roughly 58 aerosol particles in the focal zone.

The Model 3076 Constant Output Atomizer was utilized as the aerosol generation system for our research experiments. This apparatus primarily comprises a metal stand, a glass container, and a specialized atomizer assembly block, the details of which are illustrated in figure 2.1.

Compressed nitrogen ( $N_2$ ) gas was delivered to the assembly block at 30psi in our experimental setup. The gas flowed through a small opening orifice, creating a high-velocity jet. This jet was instrumental in the atomization process, as the liquid was drawn into the atomizing section due to the pressure differential created by the rapid gas flow.

The mechanism of action involved the liquid being drawn by the nitrogen gas flow towards the wall opposite the jet. Upon impact, the liquid was atomized by the force of the gas jet, forming fine droplets. Coarser droplets, unable to maintain their trajectory, fell back into the reservoir for recycling. The fine particles, however, were able to exit the atomizer through the top opening. These particles were then channeled to our setup via a PTFE tube, where measurements could be taken.

### ***2.2.b SHS Setup***

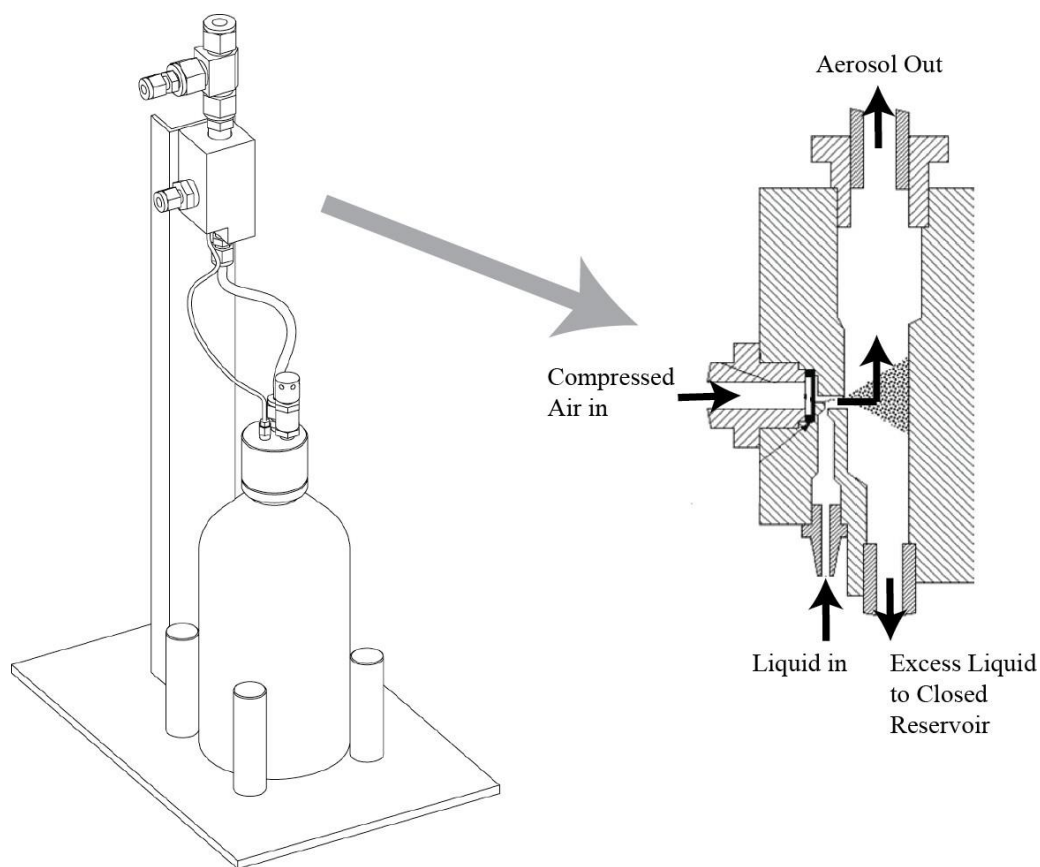
The schematic of the setup for our SHS system is shown as figure 2.2. Which has a fundamental light pulse at 800 nm were provided by a Ti: Sapphire oscillator (Coherent Micra-5, 78 MHz, 400 milliwatts, nominal pulse width 100fs). The laser beam was first passed through a 780 nm long-pass filter before being focused by a lens (focal length 50 mm; 2-inch diameter) into the aerosol sample. After the sample, the fundamental light and the SHS signal were collected by a lens (focal length 60 mm; 2-inch diameter) and subsequently focused into a monochromator by a lens (focal length 250 mm; 2-inch diameter) which matched the f-number of a homemade spectrometer. A bandpass filter (Thorlabs, FGB37S) was placed in front of the monochromator to block the fundamental 800 nm light. The signal was detected by a photomultiplier tube (PMT; Hamamatsu 4220P). The signal from the PMT was further amplified by a preamplifier (Stanford research), processed by a single photon counter (Stanford Research, SR400), and digitized by a computer through a GPIB cable.

### ***2.2.c Materials***

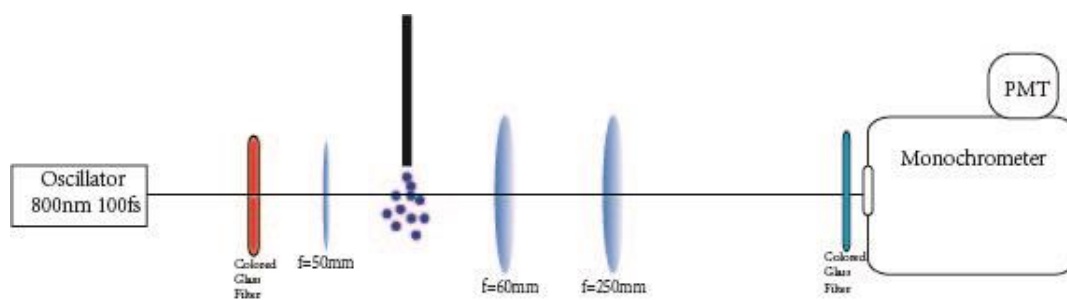
An aqueous solution of 1 M Sodium Chloride (Fisher Scientific) and 1M Ammonium Sulfate (Fisher Scientific) was prepared using distilled deionized water (>18.2 M $\Omega$ ) for use as stock solutions for the aerosol maker. Trans-4-[4-(dibutylamino)styryl]-1-methylpyridinium Iodide (DiA-4, Sigma-Aldrich) was used as received and dissolved in methanol to prepare a two millimolar solution.

Figure 2.3 shows the UV-Visible spectrum of DiA-4, a hemicyanine nonlinear chromophore known for its SHG activity. It was utilized as a probe molecule in aerosol

surfaces for subsequent SHG experiments. The absorption spectrum of DiA-4 in water at a concentration of 20  $\mu\text{M}$  exhibits a pronounced absorption peak at 475 nm, associated with S0–S1 absorption. This peak encompasses 400 nm, aligning with our SHS signal.



**Figure 2.1** Schematics of laboratory aerosol generator (Model 3076 left) and the atomizer assembly block (right)



**Figure 2.2** A schematic of second harmonic scattering experimental setup of laboratory generated aerosols.

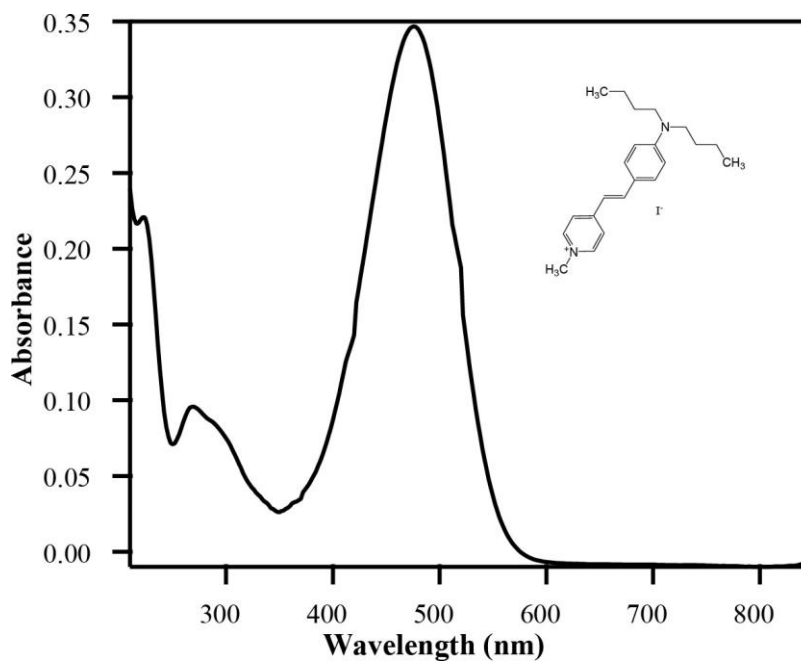


**Figure 2.3** The chemical structure of DiA-4 and corresponding UV-Visible spectrum.

### ***2.2.d Aerosol Characterization***

In our experiments, the aerosols generated by the commercial aerosol generator are distributed from tens of nanometers to several microns. Using the scanning mobility particle sizer (SMPS, TSI 3938L87), we could measure the number density of aerosol particles at different diameters. Figure 2.4(a) shows the results that the 100nm diameter aerosols are most abundant in the aerosol flow. However, Figure 2.4(b) shows that the 200nm diameter aerosols generate the strongest SHS signals. SHS intensity is proportional to the square of the number of molecules at the aerosol surface. In other words, SHS intensity is quadratic to the radius of molecules. Further calculation shows that aerosol particles with a 100nm radius (200nm diameters) will give us the highest SHS intensity. In this work, the aerosol radius in further calculations refers to 100nm.

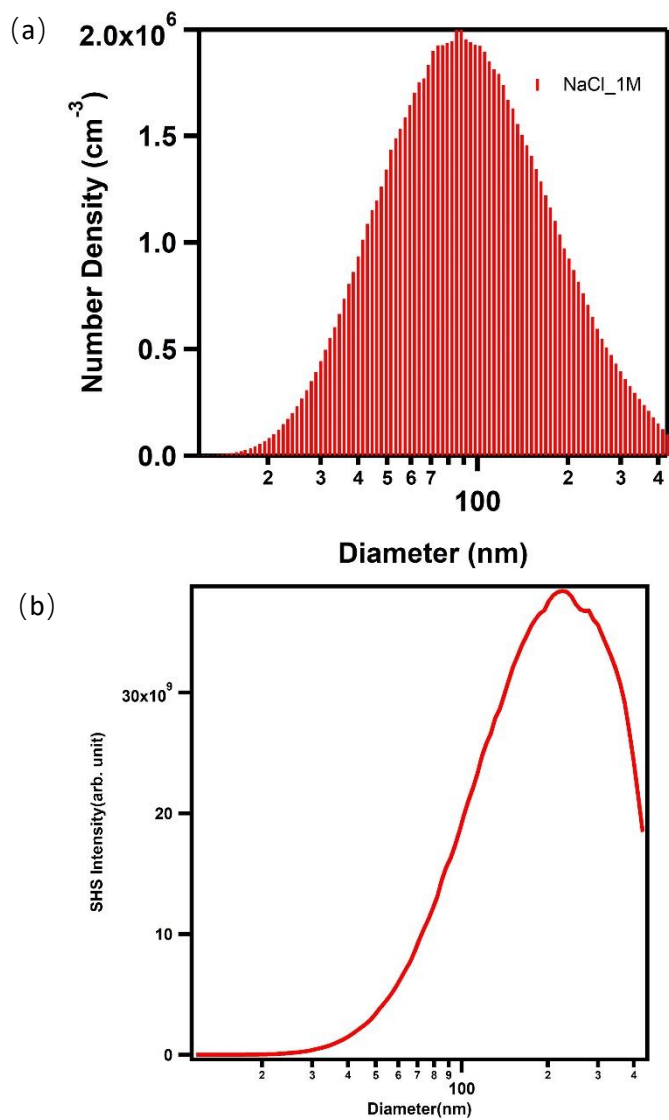
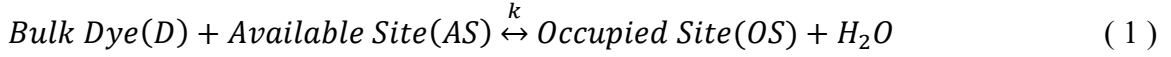


**Figure 2.4** (a) particle size measured by scanning mobility particle sizer (SMPS) and (b) corresponding SHS intensity as a function of particle diameter.

### 2.3 Fitting model

In an aerosol droplet, dye molecule equilibrium between the bulk and the surface is expressed as:



where the equilibrium constant,  $k$ , can be expressed as:

$$k = \frac{\rho_{OS} * [H_2O]}{[D] * \rho_{AS}} \quad (2)$$

where  $\rho_{OS}$  and  $\rho_{AS}$  represent the number density of occupied sites and available sites at the aerosol surface, respectively.  $[D]$  represents the DiA-4 concentration within the interior of the aerosol bulk.  $[H_2O]$  is the concentration of water, roughly 55.5 mol/L.

It is important to recognize that in aerosols, the following constraints on molecular concentrations exist:

$$[D] = ([D]_0 * V_{aerosol} * N_A - \rho_{OS} * A_{surface}) / (V_{aerosol} * N_A) \quad (3)$$

$$\rho_{AS} = N_{max} - \rho_{OS} \quad (4)$$

Where  $V_{aerosol}$  and  $A_{surface}$  are the aerosol droplets' volume and the aerosol's surface area, respectively. Here,  $[D]_0$  is the total DiA-4 concentration within an aerosol particle and is the same as the stock solution concentration used in the aerosol generator. The concentration of DiA-4 in the bulk interior of the aerosol,  $[D]$ , is defined as the difference between the total DiA-4 molecules in the aerosol and the number of DiA-4 at the surface. The maximum possible number density of DiA-4 at the aerosol surface,  $N_{max}$ , is the sum of the number density of the available and occupied surface sites. The unit of  $N_{max}$ ,  $\rho_{OS}$ , and  $\rho_{AS}$  is the number of molecules per unit area or  $\#/cm^2$ . The unit of  $[D]$ ,  $[D]_0$ , and  $[H_2O]$  is molarity, or mol/L.

Where  $V_{\text{aerosol}}$  and  $A_{\text{surface}}$  are the aerosol droplets' volume and the aerosol's surface area, respectively. Here,  $[D]_0$  is the total DiA-4 concentration within an aerosol particle and is the same as the stock solution concentration used in the aerosol generator. The concentration of DiA-4 in the bulk interior of the aerosol,  $[D]$ , is defined as the difference between the total DiA-4 molecules in the aerosol and the number of DiA-4 at the surface. The maximum possible number density of DiA-4 at the aerosol surface,  $N_{\text{max}}$ , is the sum of the number density of the available and occupied surface sites. The unit of  $N_{\text{max}}$ ,  $\rho_{\text{OS}}$ , and  $\rho_{\text{AS}}$  is the number of molecules per unit area or  $\#/\text{cm}^2$ . The unit of  $[D]$ ,  $[D]_0$ , and  $[\text{H}_2\text{O}]$  is molarity, or mol/L.

In the original formulation of the Langmuir adsorption model, the number of molecules at the surface is significantly smaller than the total available molecules in bulk; hence in Eq4, the term  $\rho_{\text{OS}} * A_{\text{surface}}$  is negligible, and  $[D]$  and  $[D]_0$  are the same. However, due to the limited volume of the aerosol particles, molecules at the surface may significantly reduce the number of molecules in bulk, and Eq4 is required. Consequently, analysis of the aerosol isotherms must include the concentration constraints, which led to a modified Langmuir fitting model for the aerosol particles.

By combining Eqns. 3-5, we obtain

$$k = \frac{\rho_{\text{OS}} * [\text{H}_2\text{O}]}{\left( \frac{[D]_0 * V_{\text{aerosol}} * N_A - \rho_{\text{OS}} * A_{\text{surface}}}{V_{\text{aerosol}} * N_A} \right) * (N_{\text{max}} - \rho_{\text{OS}})} \quad (5)$$

And derive the following expression for the number density of DiA-4 molecules at the aerosol surface  $\rho_{\text{OS}}$ :

$$\rho_{OS} = \frac{\left([D]_0 + \frac{3*N_{max}}{r*NA} + \frac{[H_2O]}{K}\right) - \sqrt{\left([D]_0 + \frac{3*N_{max}}{r*NA} + \frac{[H_2O]}{K}\right)^2 - 4*\frac{3}{r*NA}*N_{max}*[D]_0}}{2*\frac{3}{r*NA}} \quad (6)$$

The surface coverage  $\theta$  can subsequently be expressed as:

$$\theta = \frac{\rho_{OS}}{N_{max}} = \frac{\left([D]_0 + \frac{3*N_{max}}{r*NA} + \frac{[H_2O]}{K}\right) - \sqrt{\left([D]_0 + \frac{3*N_{max}}{r*NA} + \frac{[H_2O]}{K}\right)^2 - 4*\frac{3}{r*NA}*N_{max}*[D]_0}}{2*\frac{3*N_{max}}{r*NA}} \quad (7)$$

here  $\theta$  represents the surface coverage of DiA-4 molecules on the aerosol surface. DiA-4 has an absorption peak at around 475 nm and contributes to resonance enhancement of the SHG process. The SHS signal can be expressed as:

$$I_{SH} = a * \theta^2 + b * [DiA - 4] + c \quad (8)$$

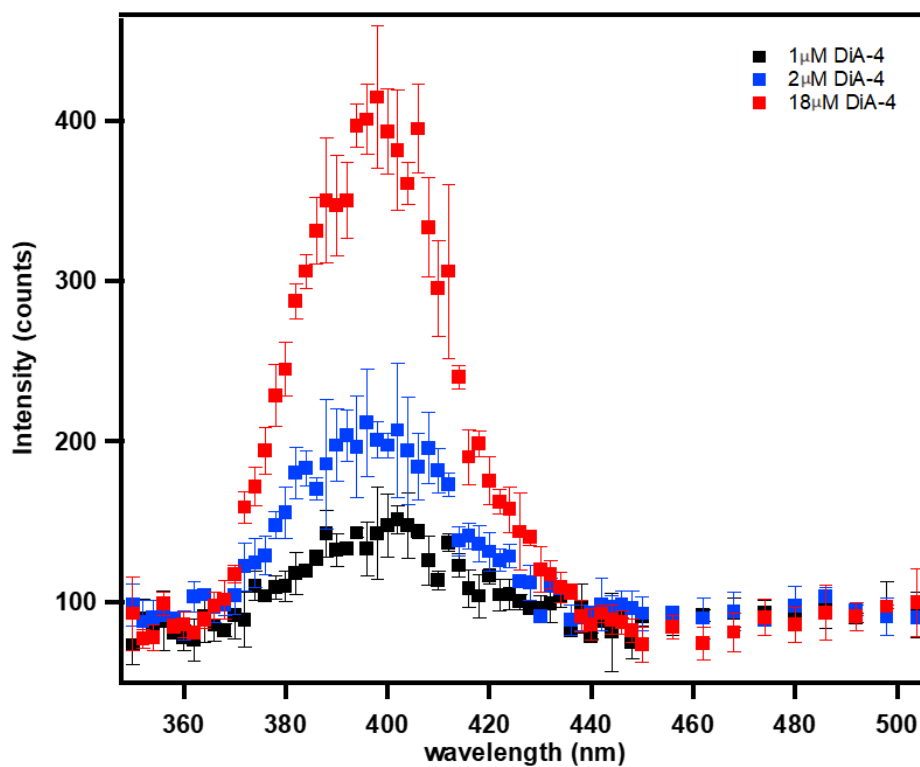
In addition to the SHS signal from the surface molecules, there could also be an incoherent hyper-Rayleigh scattering (HRS) signal contributing to the peak at 400 nm. The hyper-Rayleigh scattering may originate from all DiA-4 molecules in the aerosol. And  $c$  represents the background noise. In the first term,  $\theta$  is, in principle, determined by the Langmuir adsorption isotherm, which dictates the relationship between the surface coverage and the molecular concentration. The second linear term represents the incoherent signals from the hyper-Rayleigh scattering, which are usually negligible in planar surface experiments due to reflection geometry. However, in aerosols, both surface and bulk molecules can produce HRS due to scattering geometry. With SHS intensity being lower in aerosols, the HRS contribution to the total signal becomes significant.

## 2.4 Results and discussion

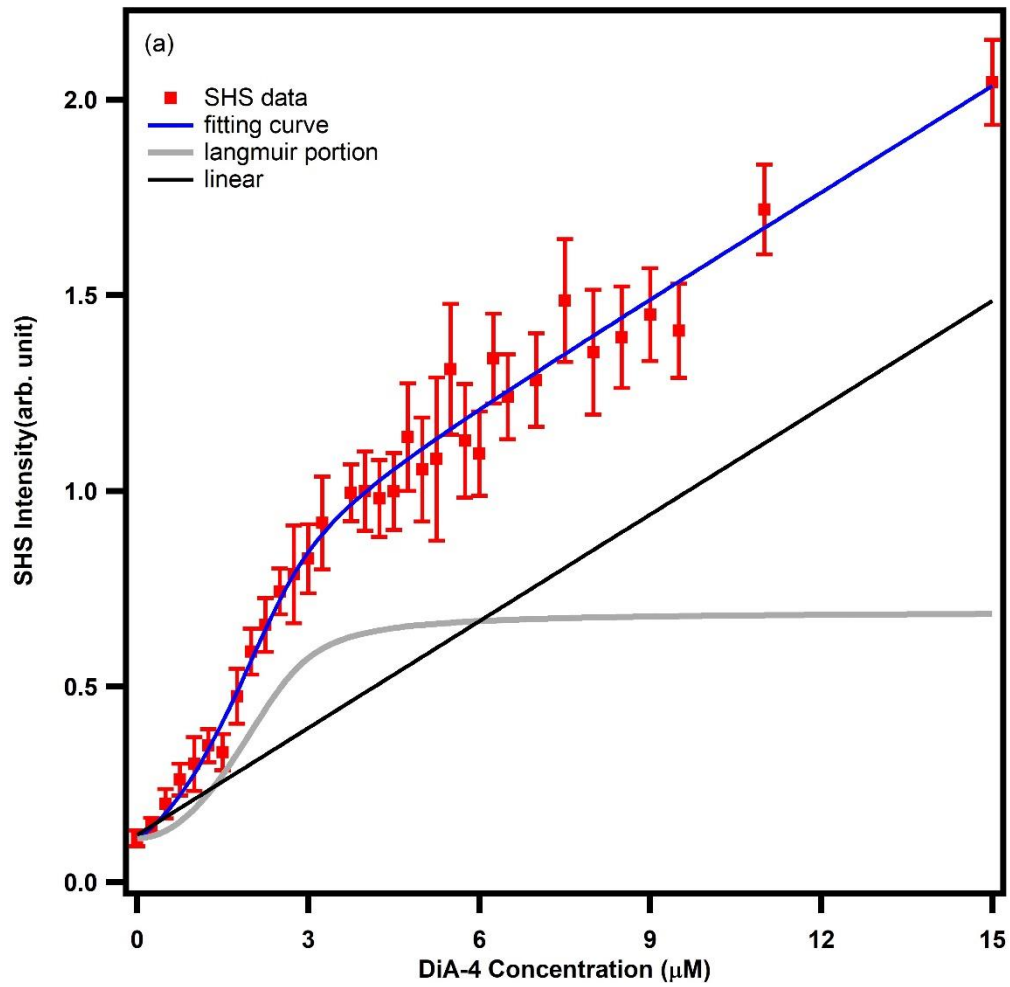
Figure 2.5 shows representative spectra of light scattered from DiA-4-containing NaCl aerosols. The peak at 400 nm is assigned to the second-harmonic scattering of the

800 nm fundamental beam. The intensity of this peak increases with DiA-4 concentration.

The integrated intensity of the 400 nm peak as a function of the concentration of DiA-4 in the two salt solutions is plotted in Figure 2.6(a) for NaCl aerosols and Figure 2.6(b) for  $(\text{NH}_4)_2\text{SO}_4$  aerosols. The red dots represent the average of three experimental measurements at each of the DiA-4 concentrations. The blue curve is the fitted result using Eqns. 1 and 8: the black line is the linear term, and the grey line is the SHS term with  $\theta$  expressed through the Langmuir fitting model. The grey line represents the coherent SHS signal from the surface DiA-4 molecules. The black linear line indicates the hyper-Rayleigh scattering which is linear to the DiA-4 concentration.



**Figure 2.5** Spectra of second harmonic scattered signal from DiA-4-containing model NaCl aerosols.



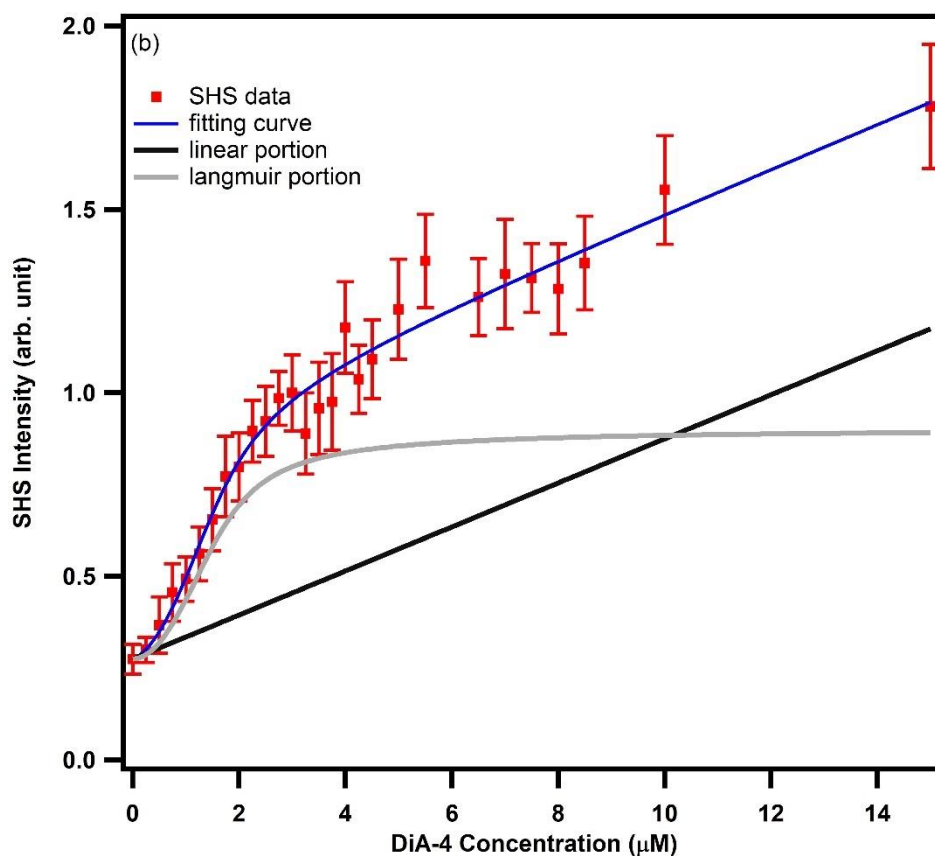


**Figure 2.6** Langmuir isotherm of SHS signal of (a) NaCl aerosols and (b)  $(\text{NH}_4)_2\text{SO}_4$  aerosols, respectively. The red dot is the original SHS signal. The blue line is the model fitting curve. The grey line represents the Langmuir contribution, and the black linear line represents the incoherent hyper-Rayleigh scattering contribution.

Fitting the Langmuir isotherms reveals  $k$  (from which the Gibbs free energy can be deduced) and the maximum number density of DiA-4 at the surface of the aerosol  $N_{\max}$ . The fitting parameters are listed in Table 2.1. The fitting results show that in NaCl aerosols, the equilibrium constant  $k$  has a value of  $(5.91 \pm 3.85) * 10^8$ , yielding Gibbs free energy  $\Delta G = -11.80 \pm 0.46$  kcal/mol. The maximum surface density of DiA-4 would be  $(5.30 \pm 0.58) * 10^9$  molecules/cm<sup>2</sup>. In (NH<sub>4</sub>)<sub>2</sub>SO<sub>4</sub> aerosols, the equilibrium constant  $k$  has a value of  $(3.94 \pm 1.99) * 10^8$ , yielding Gibbs free energy  $\Delta G = -11.63 \pm 0.33$  kcal/mol. The maximum surface density of DiA-4 would be  $(3.38 \pm 0.67) * 10^9$  molecules/cm<sup>2</sup>.

**Table 2.1** DiA-4 Maximum Number Density at the aerosol surface  $N_{\max}$  (/cm<sup>2</sup>), Equilibrium Constant  $k$ , and Gibbs Free Energy  $\Delta G$  (kCal/mol) of NaCl Aerosols and (NH<sub>4</sub>)<sub>2</sub>SO<sub>4</sub> Aerosols

	$N_{\max}(\#/cm^2)$	Equilibrium Constant $k$	Free energy $\Delta G$ (kCal/mol)
NaCl Aerosol	$(5.30 \pm 0.58) * 10^9$	$(5.91 \pm 3.85) * 10^8$	$-11.80 \pm 0.46$
(NH <sub>4</sub> ) <sub>2</sub> SO <sub>4</sub> Aerosol	$(3.38 \pm 0.67) * 10^9$	$(3.94 \pm 1.99) * 10^8$	$-11.63 \pm 0.33$

Notably, the maximum surface density observed at the aerosol surface is roughly five orders of magnitude lower than that reported on polystyrene particle surfaces and the flat air-water interface, which approximates  $\sim 10^{13}$  molecules/cm<sup>2</sup>.(12) This discrepancy in surface density arises primarily from overlooking constraints presented by Eq3 and Eq4. One must recognize that aerosols have a significantly limited supply of organic molecules. In contrast, for colloidal particles in solutions, there's an abundance of organic molecules available to occupy the polystyrene particle surface sites. In the case of flat surfaces, the molecular supply in the bulk appears virtually infinite compared to the molecules at the air-water interface. Therefore, while the Langmuir fitting for the flat

surface model assumes a vast excess of molecules in the bulk over those at the interface, such an assumption is inapplicable to the aerosol scenario.

With the fitting parameters, maximum surface DiA-4 concentration, and the equilibrium constant, we can calculate the DiA-4 molecules partitions at the aerosol surface.

$$\begin{aligned} \text{DiA-4 surface partition} &= \frac{\rho_{OS} * A_{\text{surface}}}{[D]_0 * V_{\text{aerosol}} * N_A} \\ &= \frac{\left([D]_0 + \frac{3 * N_{\text{max}}}{r * N_A} + \frac{[H_2O]}{K}\right) - \sqrt{\left([D]_0 + \frac{3 * N_{\text{max}}}{r * N_A} + \frac{[H_2O]}{K}\right)^2 - 4 * \frac{3}{r * N_A} * N_{\text{max}} * [D]_0}}{2 * [D]_0} \end{aligned} \quad (10)$$

Eq 10 is used to calculate the partition of DiA-4 molecules at the aerosol surface. Figure 2.7(a) depicts the surface partition of DiA-4 at varying total concentrations. The x-axis is presented in a logarithmic scale to emphasize the low-concentration region. The red and blue plots represent surface partitions at NaCl and (NH<sub>4</sub>)<sub>2</sub>SO<sub>4</sub> aerosol surfaces, respectively. The figure illustrates that when the concentration of the organic molecule DiA-4 is below 1 μM, over 90% of the molecules are located at the surface of both types of aerosols. Moreover, the surface partition of DiA-4 is higher in NaCl aerosols compared to (NH<sub>4</sub>)<sub>2</sub>SO<sub>4</sub> aerosols. As the concentration of water-soluble organic molecules increases, the aerosol surface becomes saturated, compelling more molecules into the aerosol's aqueous interior. This results in a reduced surface partition at high DiA-4 concentrations.

Figure 2.7(b) illustrates that as the particle size increases, a greater number of molecules remain in the bulk, resulting in reduced surface partitioning. This phenomenon

is attributed to the decrease in the surface-to-volume ratio. This observation underscores the significance of reexamining the air-water interface of aerosol droplets. Smaller droplets exhibit higher molecule partitioning at the aerosol surface, emphasizing the increasing importance of surface properties in aerosols as their size diminishes.

## **2.5 Conclusion**

In summary, our research showcases the use of Second Harmonic Scattering (SHS) as an effective approach to study the partitioning behavior of water-soluble organic molecules at the aerosol surface. We employed the hemicyanine dye, DiA-4, as a model water-soluble organic molecule to analyze its concentration-dependent surface coverage in lab-generated NaCl and  $(\text{NH}_4)_2\text{SO}_4$  aerosols. Our data demonstrate that the majority of water-soluble organic molecules localize to the aerosol surface at lower organic molecule concentrations, thereby highlighting the importance of aerosol surface properties in photoreactions.

Our findings bear significant implications for comprehending the physical and chemical properties of atmospheric aerosols, particularly the partitioning of water-soluble organic molecules at the aerosol surface. This knowledge furthers our understanding of atmospheric processes like cloud formation, radiation balance, and air quality.

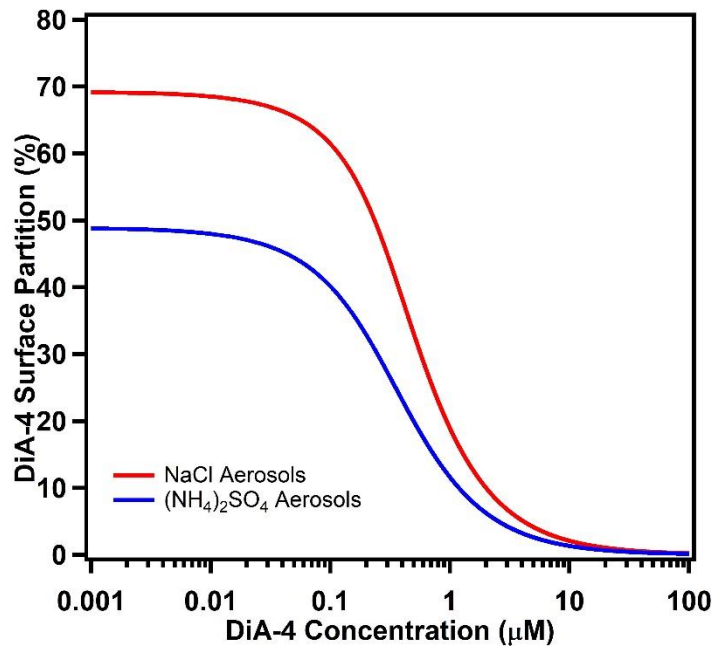
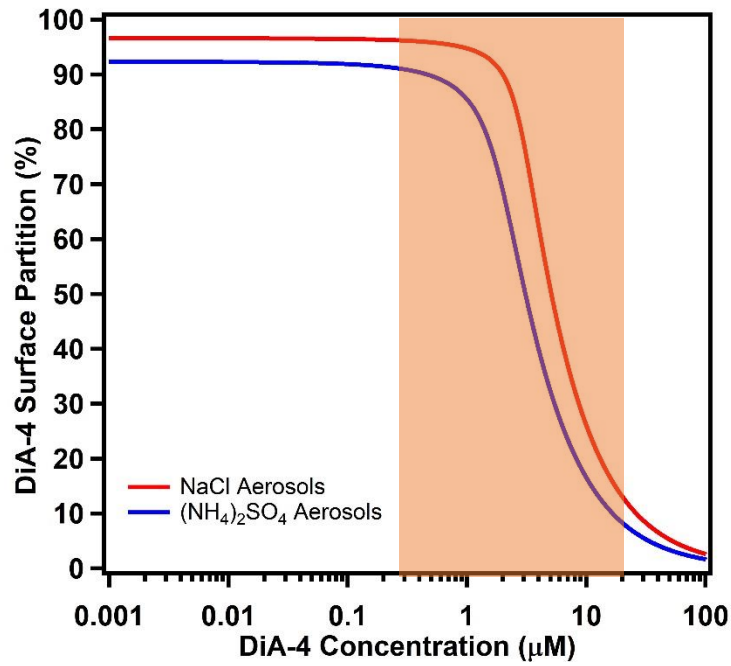


**Figure 2.7** DiA-4 partition at aerosol surface of (a) 100nm radius aerosols and (b) 2.5 $\mu\text{m}$  diameter aerosols (PM 2.5). The shaded area is the experimental concentration.

## 2.6 Bibliography

1. Valsaraj, K. T. A Review of the Aqueous Aerosol Surface Chemistry in the Atmospheric Context. *Open Journal of Physical Chemistry* **2012**, *02*(01), 58–66. doi:10.4236/ojpc.2012.21008.
2. Bluhm, H.; Siegmann, H. C. Surface science with aerosols. *Surface Science* **2009**, *603*(10–12), 1969–1978. doi:10.1016/j.susc.2008.08.041.
3. Bao, H.; Niggemann, J.; Luo, L.; Dittmar, T.; Kao, S. J. Molecular composition and origin of water-soluble organic matter in marine aerosols in the Pacific off China. *Atmospheric Environment* **2018**, *191*(December 2017), 27–35. doi:10.1016/j.atmosenv.2018.07.059.
4. Xie, M.; Mladenov, N.; Williams, M. W.; Neff, J. C.; Wasswa, J.; Hannigan, M. P. Water soluble organic aerosols in the Colorado Rocky Mountains, USA: Composition, sources and optical properties. *Scientific Reports* **2016**, *6*. doi:10.1038/srep39339.
5. Laimgruber, S.; Schachenmayr, H.; Schmidt, B.; Zinth, W.; Gilch, P. A femtosecond stimulated raman spectrograph for the near ultraviolet. *Applied Physics B: Lasers and Optics* **2006**, *85*(4), 557–564. doi:10.1007/s00340-006-2386-8.
6. Graham, B.; Mayol-Bracero, O. L.; Guyon, P.; Roberts, G. C.; Decesari, S.; Facchini, M. C.; et al. Water-soluble organic compounds in biomass burning aerosols over Amazonia 1. Characterization by NMR and GC-MS. *Journal of Geophysical Research Atmospheres* **2002**, *107*(20), LBA 14-1-LBA 14-16. doi:10.1029/2001JD000336.
7. Nájera, J. J.; Horn, A. B. Infrared spectroscopic study of the effect of oleic acid on the deliquescence behaviour of ammonium sulfate aerosol particles. *Physical Chemistry Chemical Physics* **2009**, *11*(3), 483–494. doi:10.1039/b812182f.
8. Shen, Y. Optical Second Harmonic Generation At Interfaces. *Annual Review of Physical Chemistry* **1989**, *40*(1), 327–350. doi:10.1146/annurev.physchem.40.1.327.
9. Gonella, G.; Dai, H. L. Second harmonic light scattering from the surface of colloidal objects: Theory and applications. *Langmuir* **2014**, *30*(10), 2588–2599. doi:10.1021/la403570f.

10. Wu, Y.; Li, W.; Xu, B.; Li, X.; Wang, H.; McNeill, V. F.; et al. Observation of Organic Molecules at the Aerosol Surface. *Journal of Physical Chemistry Letters* **2016**, *7*(12), 2294–2297. doi:10.1021/acs.jpcllett.6b00872.
  
11. Kim, J. Excited-state photophysics and dynamics of a hemicyanine dye in AOT reverse micelles. *Journal of Physical Chemistry A* **1999**, *103*(18), 3378–3382. doi:10.1021/jp984167e.
  
12. Wang, H.; Troxler, T.; Yeh, A. G.; Dai, H. L. In situ, nonlinear optical probe of surfactant adsorption on the surface of microparticles in colloids. *Langmuir* **2000**, *16*(6), 2475–2481. doi:10.1021/la9909087.

# CHAPTER 3 ALT IMPACT ON PARTITIONING

## DYNAMICS OF WATER-SOLUBLE

## ORGANIC MOLECULES IN AEROSOL SURFACE

### CHEMISTRY

#### 3.1 Introduction

Aerosols are a significant area of atmospheric research due to their multifaceted origins and diverse environmental impact. Based on their sources, they can be categorized primarily into sea salt and urban aerosols. While sea-salt aerosols are derived from oceanic processes, urban aerosols have a mixed origin, with significant contributions from human activities, like cooking and vehicular emissions, as well as natural processes, including volcanic eruptions and plant-based emissions.<sup>(1–3)</sup>

Given the diverse sources of aerosols, their chemical compositions are expected to vary. Beyond the evident differences in organic compounds, there are noticeable variations in the inorganic components, too. Urban aerosols, for example, often contain compounds like ammonium sulfate, ammonium nitrate, and ammonium chloride, reflecting the diverse environmental constituents in urban areas.

The optical properties of aerosols have been studied by various researchers. The scattering and absorption properties of aerosols, which in turn influence their radiative forcing, can be significantly modulated by their content. Another avenue of research has been the interaction between aerosols and other atmospheric entities. For example, the

uptake of volatile organic compounds (VOCs) by aerosols has implications for urban smog and haze formation.(4,5)

Aerosol hygroscopicity, which directly influences the cloud nucleation properties of particles, is largely modulated by their salt content. Salts in aerosols can absorb moisture, leading to particle growth and potentially affecting the light scattering properties. Further, some inorganic salts in aerosols can undergo reactions in the presence of specific atmospheric species, leading to the formation of new particle phases or influencing particle morphology.(6,7)

Researchers have been keen to understand the role of salts in modulating properties of aqueous solutions. The Hofmeister series is a notable concept in this domain. It essentially ranks ions based on their ability to affect protein solubility.(8) Although this series has been invaluable in understanding solubility dynamics, the exact mechanisms underpinning the observed effects remain a subject of ongoing research.

Dr. Tobias's work on Molecular Dynamic (MD) simulations offers intriguing insights into the behavior of ions at the air-water interface. By simulating different salt environments, he observed the differential distribution of ions near this interface.(9) Such studies help underscore the complexity of interactions at aerosol surfaces, particularly when considering diverse salt compositions.

In this chapter, we will delve deeper into the intricacies of the aerosol air-water interface, focusing on its response to varying salt compositions. By experimenting with different salts, I aimed to understand their impact on the distribution of water-soluble organics on the aerosol surface. My study involved salts such as NaCl,  $(\text{NH}_4)_2\text{SO}_4$ ,  $\text{NH}_4\text{Cl}$ , and  $\text{NH}_4\text{NO}_3$ . Initial findings indicate that the type of anions in salts can significantly influence the positioning of organic molecules on aerosol surfaces. For instance, aerosols with  $\text{SO}_4^{2-}$  ions showed reduced organic surface concentrations compared to those with  $\text{Cl}^-$  ions.

Our findings align closely with the molecular dynamics (MD) simulation outcomes from the Tobias group, providing compelling evidence of ions significantly impacting the properties of the air-water interface, particularly on aerosol surfaces. These results underscore that aerosol surface properties can differ based on their composition and origin, leading to variations in how organic molecules partition on the aerosol surfaces. Consequently, the capability of aerosols to adsorb organic molecules from their surroundings varies, influenced by the location and source of the primary aerosols.

### **3.2 Experiment**

As previously described, we used second harmonic scattering experiments to measure the laboratory generated aerosols with aerosol generator (TSI 3076). The stock solution for aerosol generation is made with salt dissolved in water (HPLC level). 1M stock solution of  $(\text{NH}_4)_2\text{SO}_4$ ,  $\text{NH}_4\text{Cl}$ , and  $\text{NH}_4\text{NO}_3$  was prepared with corresponding salt from different distributors. The aerosol was generated by the aerosol generator and

directly measured with our SHS setup. As previously demonstrated, the 800nm laser beam was focused inside the aerosol column and generated detectable SHS signals from dye molecules (DiA-4, Sigma-Aldrich) on the aerosol surface. The signal was collimated by a 2-inch focusing lens and refocused by another 2-inch lens which matched the monochromator f-number. The signal was detected by a PMT (Hamamatsu 4220P) and amplified by a preamplifier (Stanford Research), then processed with a single photon counter (Stanford Research, SR410). Details can be found in the previous chapter.

### **3.3 Results and discussion**

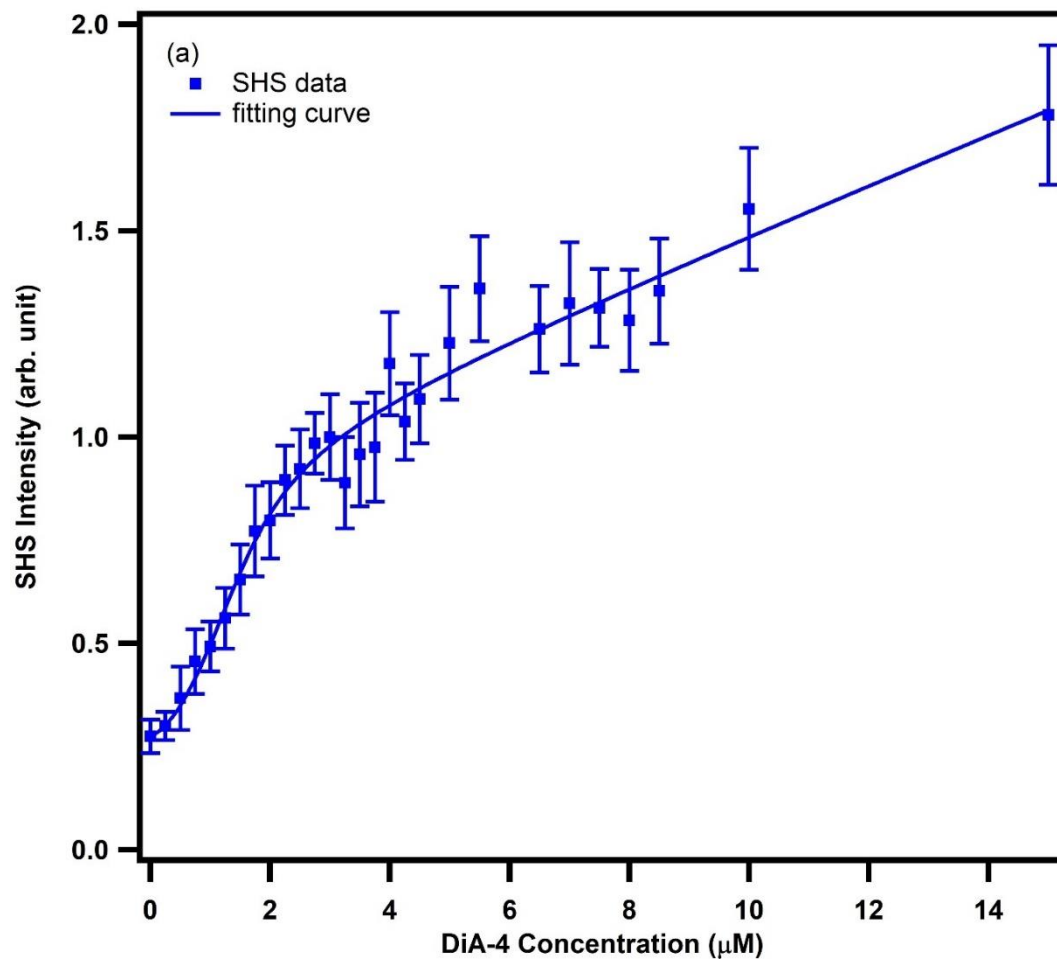
The fitting parameters for various salt aerosols are summarized in Table 3.1. This table reveals that aerosols containing different salts exhibit distinct surface properties, which in turn influence the partitioning of water-soluble organic molecules at the aerosol surface. Given that DiA-4 is a cation, the counter ion plays a crucial role in this comparison. The results indicate that aerosols with chloride ions ( $\text{Cl}^-$ ) possess the highest molecular surface density, whereas those with sulfate ions ( $\text{SO}_4^{2-}$ ) exhibit the lowest.

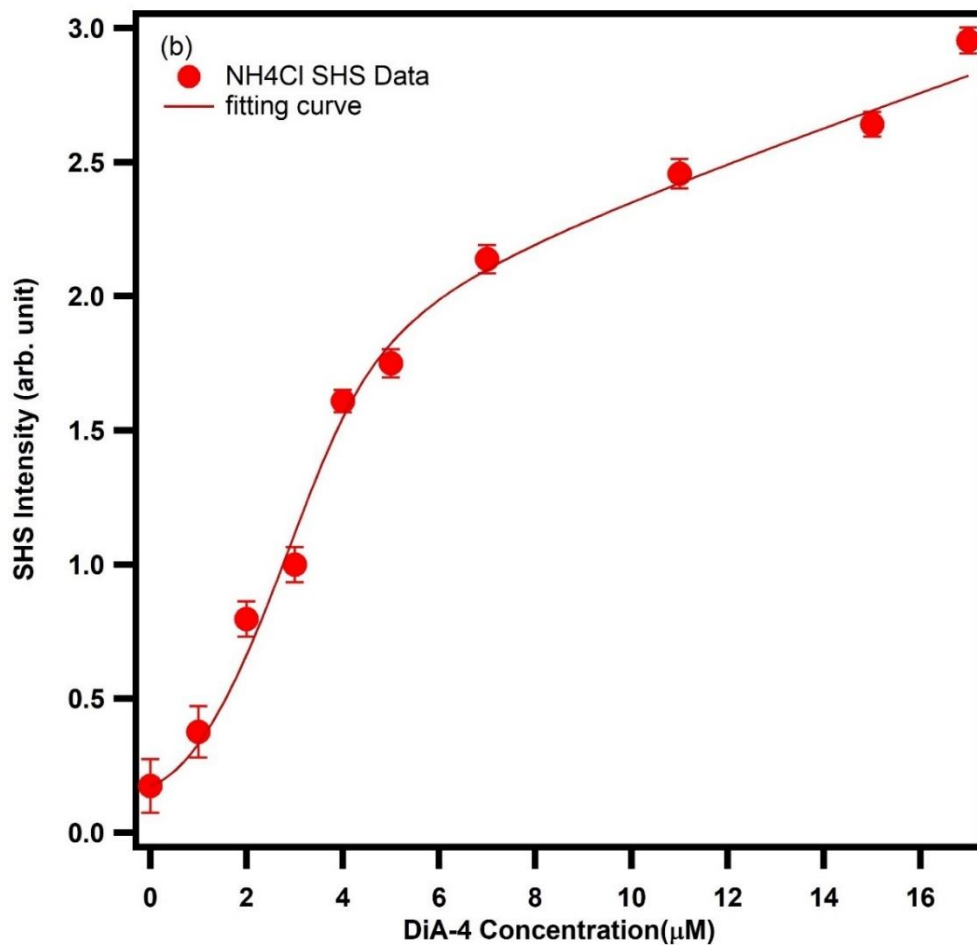
In terms of the equilibrium constant, the values for all salts are within the same order of magnitude, suggesting comparable Gibbs free energy across these systems. The Hofmeister series, which ranks ions based on their salting out or salting in effects, is derived from extensive experimental data. The theoretical basis for this series is still a topic of active debate. According to the series, sulfate ions exert the strongest effect, while chloride and nitrate ions are positioned roughly in the middle, with chloride ions

demonstrating slightly stronger effects than nitrate ions. Our findings are in remarkable agreement with the predictions of the Hofmeister series.

Considering the ionic strength of different salt solutions at the same concentration (1M in our experiments), the solution with ammonium sulfate ( $(\text{NH}_4)_2\text{SO}_4$ ) exhibits the strongest ionic strength. The ionic strengths of the other three solutions are comparable. This variance in ionic strength could be a factor in retaining DiA-4 ions within the bulk phase, resulting in reduced surface molecular density.

Literature reviews, including works by Tobias and colleagues, have extensively explored the molecular dynamics simulations of the air-water interface.<sup>(10,11)</sup> As you may see in figure 3.2, these studies have shown that ions can significantly alter the properties of the air-water interface. From figure 3.2(a) and (b), it was discovered that under the same anion chloride condition, ammonium ( $\text{NH}_4^+$ ) ions are positioned closer to the surface than chloride ( $\text{Cl}^-$ ) ions. From Figure 3.2(b) and (c), with ammonium as the cation, sulfate ( $\text{SO}_4^{2-}$ ) ions tend to pull the  $\text{NH}_4^+$  ions further into the bulk, several Angstroms deeper than chloride ions. This notable difference in cation positioning at the air-water interface aligns with our findings. Our results indicate the highest surface





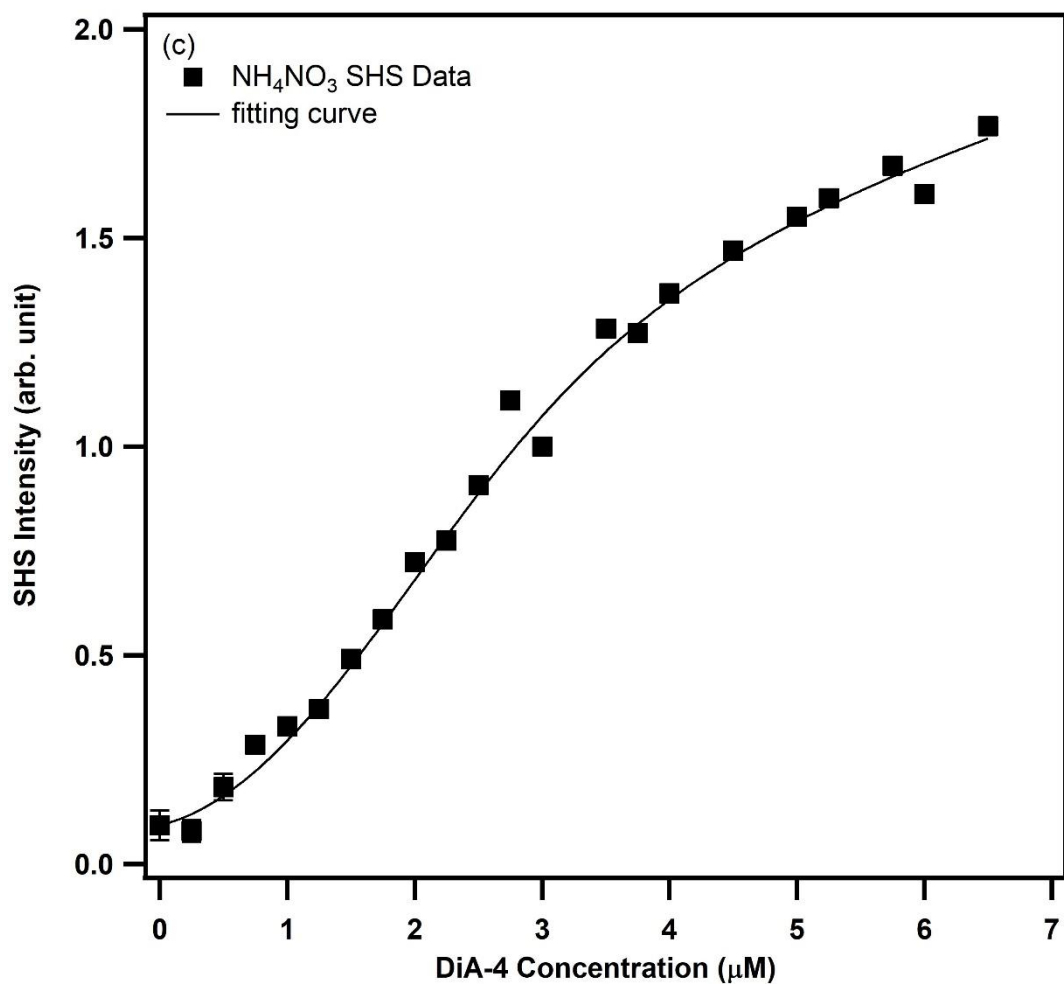


**Figure 3.1** Langmuir isotherm of SHS signal and corresponding fitting curve of a)  $(\text{NH}_4)_2\text{SO}_4$  aerosols, b)  $\text{NH}_4\text{Cl}$  aerosols, and c)  $\text{NH}_4\text{NO}_3$ , respectively.

**Table 3.1** Langmuir model fitting parameters of aerosols with different salts.

	$N_{\max}(10^9/\text{cm}^2)$	k	$\Delta G(\text{kcal/mol})$
NaCl	$5.30 \pm 0.58$	$5.91 \pm 3.9 * 10^8$	$-11.80 \pm 0.46$
$(\text{NH}_4)_2\text{SO}_4$	$3.38 \pm 0.67$	$3.94 \pm 2.0 * 10^8$	$-11.63 \pm 0.33$
$\text{NH}_4\text{Cl}$	$7.87 \pm 0.75$	$3.53 \pm 1.5 * 10^8$	$-11.59 \pm 0.27$
$\text{NH}_4\text{NO}_3$	$5.63 \pm 0.03$	$1.83 \pm 0.02 * 10^8$	$-11.26 \pm 0.01$

density of DiA-4 cations at the  $\text{NH}_4\text{Cl}$  aerosol air-water interface, followed by NaCl, with the lowest in  $(\text{NH}_4)_2\text{SO}_4$ . This trend is consistent with Dr. Tobias's calculations and suggests the need for further research to validate these observations.

### 3.4 Conclusion

Our study offers significant insights into the dynamics of salt effects on the partitioning of organic molecules at aerosol surfaces, shedding light on a crucial aspect of atmospheric chemistry. Through our analysis, we found that different salts, representative of diverse aerosol sources, distinctly influence the surface behavior of aerosols. Notably, sodium chloride, a proxy for sea salt aerosols, and ammonium sulfate, representative of urban aerosols, demonstrate how variations in inorganic components can alter aerosol surface properties. These findings highlight that the geographical origin and environmental context of aerosols - whether marine or urban - crucially impact their chemical nature.

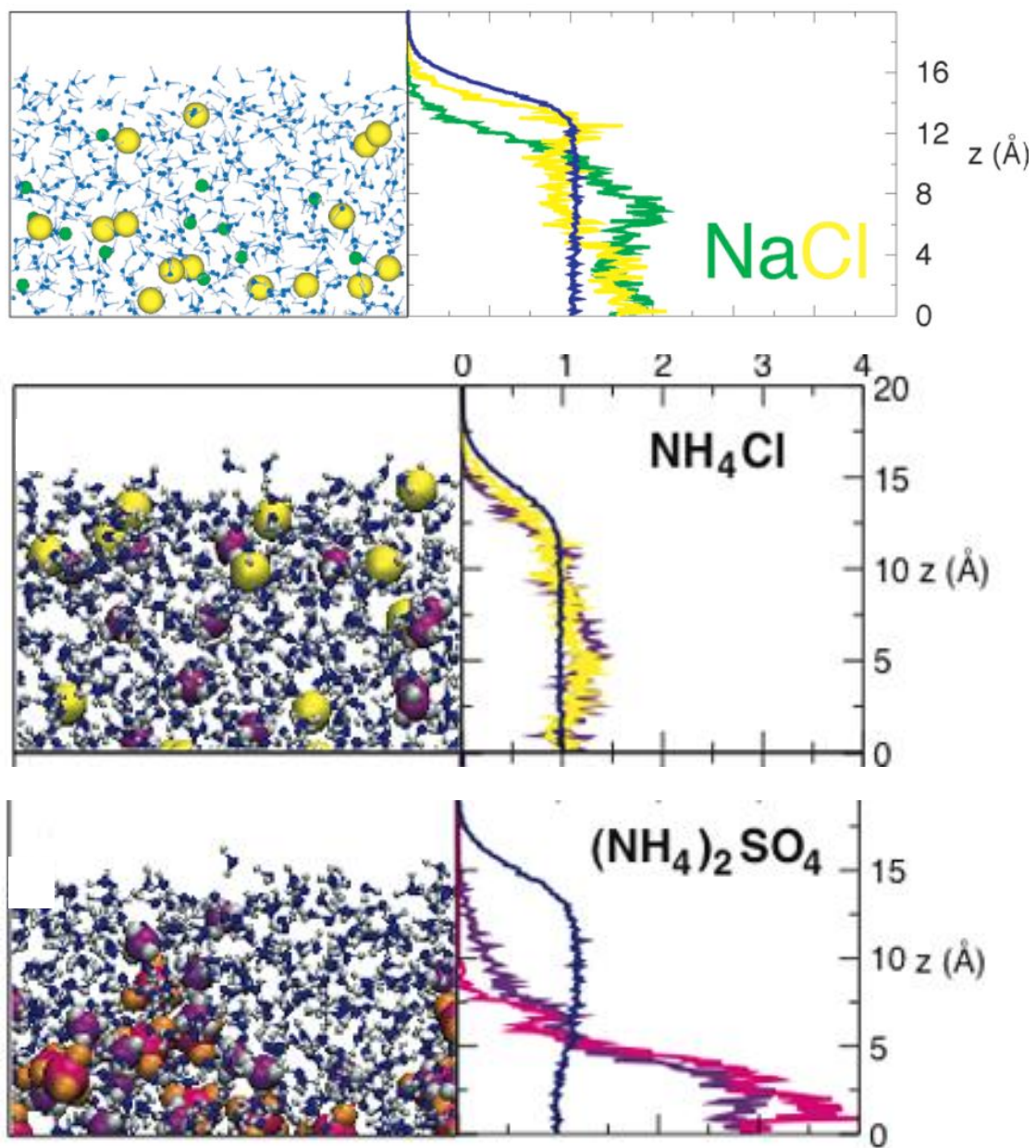


**Figure 3.2** MD simulation results of air-water interface with different salts from Dr. Tobias publications. Left: snapshot from MD results. Right: density profiles of salt ions and water oxygens from the center of the slab ( $z = 0$ ) to the air/ water interface.

The contrasting behavior of sulfate and chloride ions, as elucidated in our study and supported by molecular dynamics simulations, underscores the nuanced influence of salt composition on the atmospheric behavior of aerosols. This difference is particularly significant when considering the real-world implications, where the prevalent aerosol type in a region could affect atmospheric processes and environmental conditions. By correlating our empirical observations with the Hofmeister series, we provide a deeper understanding of how ionic strength and ion positioning at the air-water interface contribute to aerosol surface chemistry. These insights not only enhance our comprehension of the intricate mechanisms governing atmospheric processes but also offer valuable perspectives for future research aimed at addressing environmental challenges related to aerosol behavior and air quality.

### 3.5 Bibliography

1. Salvo, A.; Brito, J.; Artaxo, P.; Geiger, F. M. Reduced ultrafine particle levels in São Paulo's atmosphere during shifts from gasoline to ethanol use. *Nature Communications* **2017**, *8*(1), 1–13. doi:10.1038/s41467-017-00041-5.
2. Patterson, J. P.; Collins, D. B.; Michaud, J. M.; Axson, J. L.; Sultana, C. M.; Moser, T.; et al. Sea spray aerosol structure and composition using cryogenic transmission electron microscopy. *ACS Central Science* **2016**, *2*(1), 40–47. doi:10.1021/acscentsci.5b00344.
3. Mohimani, H.; Gurevich, A.; Mikheenko, A.; Garg, N.; Nothias, L.-F.; Ninomiya, A.; et al. Characterization of water-soluble organic matter in urban aerosol by 1 H-NMR spectroscopy. *Physiology & behavior* **2017**, *176*(3), 139–148. doi:10.1016/j.atmosenv.2015.12.067.Characterization.

4. Simon, V.; Luchetta, L.; Torres, L. Estimating the emission of volatile organic compounds (VOC) from the French forest ecosystem. *Atmospheric Environment* **2001**, *35*(SUPPL. 1). doi:10.1016/s1352-2310(00)00565-3.
5. Novak, G. A.; Bertram, T. H. Reactive VOC Production from Photochemical and Heterogeneous Reactions Occurring at the Air-Ocean Interface. *Accounts of Chemical Research* **2020**, *53*(5), 1014–1023. doi:10.1021/acs.accounts.0c00095.
6. Fletcher, C. A.; Johnson, G. R.; Ristovski, Z. D.; Harvey, M. Hygroscopic and volatile properties of marine aerosol observed at Cape Grim during the P2P campaign. *Environmental Chemistry* **2007**, *4*(3), 162–171. doi:10.1071/EN07011.
7. Frossard, A. A.; Li, W.; Gérard, V.; Nozière, B.; Cohen, R. C. Influence of surfactants on growth of individual aqueous coarse mode aerosol particles. *Aerosol Science and Technology* **2018**, *52*(4), 459–469. doi:10.1080/02786826.2018.1424315.
8. Hyde, A. M.; Zultanski, S. L.; Waldman, J. H.; Zhong, Y. L.; Shevlin, M.; Peng, F. General Principles and Strategies for Salting-Out Informed by the Hofmeister Series. *Organic Process Research and Development* **2017**, *21*(9), 1355–1370. doi:10.1021/acs.oprd.7b00197.
9. Jungwirth, P.; Tobias, D. J. Specific ion effects at the air/water interface. *Chemical Reviews* **2006**, *106*(4), 1259–1281. doi:10.1021/cr0403741.
10. Gopalakrishnan, S.; Jungwirth, P.; Tobias, D. J.; Allen, H. C. Spectroscopic and Molecular Dynamics Studies. **2005**, No. 2, 8861–8872.
11. Knipping, E. M.; Lakin, M. J.; Foster, K. L.; Jungwirth, P.; Tobias, D. J.; Gerber, R. B.; et al. Experiments and simulations of ion-enhanced interfacial chemistry on aqueous NaCl aerosols. *Science* **2000**, *288*(5464), 301–306. doi:10.1126/science.288.5464.301.

# CHAPTER 4 COMPARATIVE ANALYSIS OF CURVED AEROSOL AND PLANAR AIR-WATER INTERFACES

## 4.1 Introduction

The intricate study of surface properties plays a crucial role in atmospheric chemistry, shaping our understanding of various environmental and chemical processes. This chapter focuses on the comparative analysis of aerosol surfaces and flat air-water interfaces, two distinct yet fundamentally important phenomena in the field.

Surface chemistry, traditionally studied on flat air-water interfaces, has provided a wealth of knowledge about molecular interactions and dynamics at these interfaces.<sup>(1)</sup> Techniques such as surface tension measurements, spectroscopic methods, and molecular dynamics simulations have been instrumental in shedding light on the behavior of molecules at these surfaces.<sup>(2–4)</sup> These insights have been critical in understanding phenomena like surface adsorption, chemical reactivity, and the formation of surface films.

However, the world of aerosol surfaces presents a contrasting landscape. Aerosols, with their microscopic droplets or particles suspended in the atmosphere, offer a high surface-to-volume ratio and a unique curvature that significantly influences their surface properties.<sup>(5)</sup> The study of aerosols is not only crucial for understanding atmospheric chemistry but also for their impact on climate change, air quality, and health. The dynamic nature of aerosol surfaces, influenced by factors such as particle size,

composition, and ambient conditions, presents a complex scenario that differs markedly from the more stable flat air-water interfaces.

Thus, the need to understand the differences between these two types of surfaces emerges not just from a scientific curiosity but from a pressing need to address broader environmental and health-related issues. The contrasting behaviors of aerosol and flat surfaces have profound implications in atmospheric chemistry, influencing everything from cloud formation and precipitation to the transport and fate of pollutants in the environment.<sup>(6)</sup>

This chapter aims to delve into these contrasting worlds, exploring the differences in surface properties, reaction kinetics, and thermodynamic behaviors of aerosol surfaces compared to flat air-water interfaces. By doing so, it seeks to contribute to the broader discourse on atmospheric chemistry and environmental science, providing insights that could guide future research in these critical areas.

## **4.2 Experiments**

The aerosol experiments are the same as previously described. The planar surface second harmonic experiments use a reflection geometry, as shown in figure 4.1. The solution sample is placed in a Teflon dish and fixed on a holder which is attached onto the breadboard. The beam is focused by a 1-inch lens ( $f=15\text{cm}$ ) and collected with a lens with the same diameter and focal length. Before the lens, there is a halfwave plate and a polarizer pair to control the polarization of the beam. The signal beam is focused into the spectrometer (CM110, Spectral Product) and collected by the same PMT.

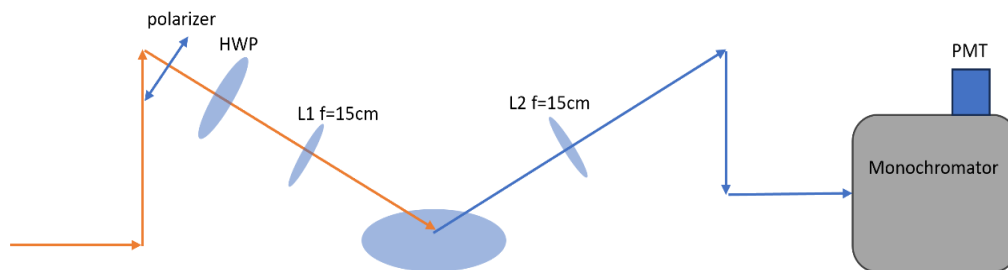


**Figure 4.1** A schematic of second harmonic generation experimental setup for planar surface

### 4.3 Results and discussion

Our experimental investigation focused on discerning the dynamic equilibrium of organic molecules, particularly dye molecules, between the bulk water phase and the air-water interface. We utilized the Langmuir adsorption model as our theoretical framework, enabling us to meticulously analyze the rate constants of molecular migration in various scenarios.

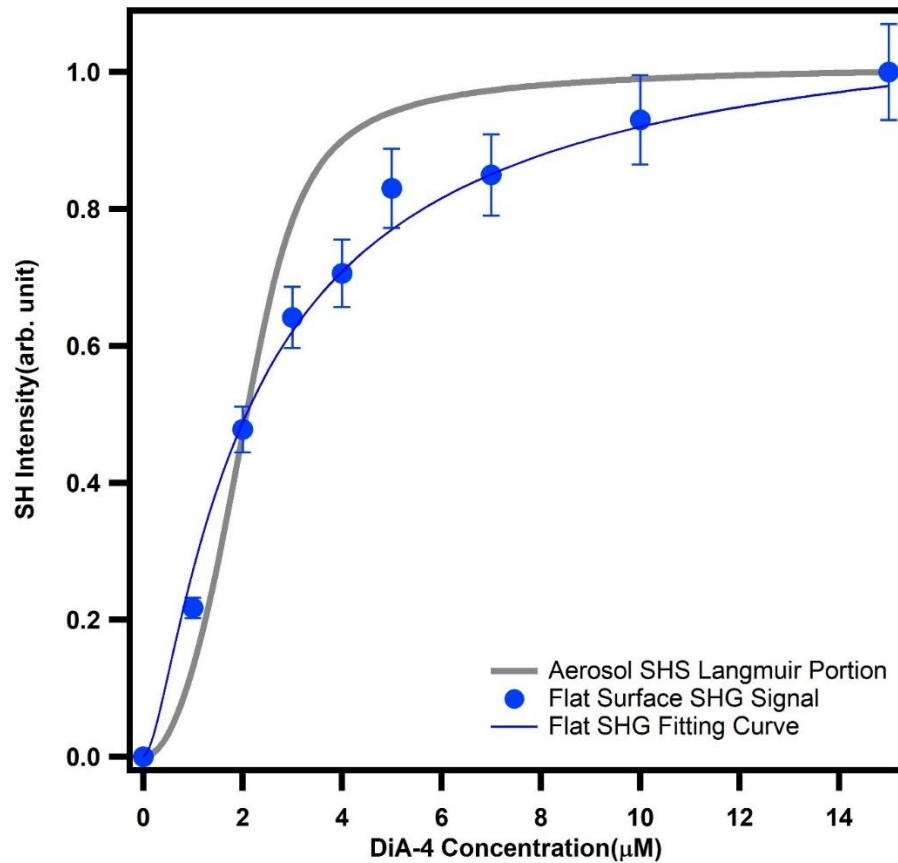
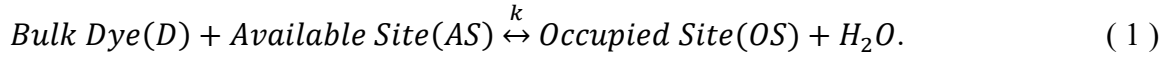


**Figure 4.2** Comparison of SHS signal of 1M NaCl aerosols (grey) and SHG signals of 1M NaCl solution air-water interface. Blue solid line is the Langmuir fitting curve of the flat surface SHG signal.

The derivation of Langmuir fitting model is as below:



where the equilibrium constant, k, can be expressed as:

$$k = \frac{[OS]*[H_2O]}{[D]*[AS]} \quad (2)$$

$$[D] = [D]_0 - [OS] \approx [D]_0 \quad (3)$$

$$[AS] = N_{max} - [OS] \quad (4)$$

In this case, the bulk supply of dye molecules is infinite, in other words,  $[D]_0$  is much larger than  $[OS]$ . When we neglect  $[OS]$  term in equation 3, we get  $[D] = [D]_0$ . Now we can get:

$$k = \frac{[OS]*[H_2O]}{[D]_0*(N_{max} - [OS])} \quad (5)$$

We can now get the expression of  $[OS]$ :

$$[OS] = \frac{N_{max}*[D]_0*k}{[H_2O] + [D]_0*k} \quad (6)$$

The surface coverage can be expressed as:

$$\theta = \frac{[OS]}{N_{max}} = \frac{[D]_0*k}{[H_2O] + [D]_0*k} \quad (7)$$

In the surface coverage expression, we can only get equilibrium constant k and the maximum surface number density  $N_{max}$  is cancelled out during the calculation.

**Table 4.1** Rate constant  $k$  of aerosol and flat air-water interface with corresponding Gibbs free energy  $\Delta G$ .

	Equilibrium constant $k$	Gibbs free energy $\Delta G$ (kcal/mol)
Aerosol fitting	$5.91 \pm 3.85 * 10^8$	$-11.80 \pm 0.46$
Flat surface fitting	$5.41 \pm 0.41 * 10^7$	$-10.54 \pm 0.04$

When normalizing the Second Harmonic Scattering (SHS) signal from 1M NaCl aerosols and the Second Harmonic Generation (SHG) signals from a 1M NaCl solution at the air-water interface, it becomes apparent that the molecular equilibrium between the bulk and the air-water interface differs in these two scenarios. This is due to the significant depletion of molecules in the bulk phase in the aerosol scenario. It's important to note that a modified Langmuir model was applied to the aerosol case, while the standard Langmuir model was used for the flat air-water interface. In the Langmuir fitting model, equations eliminate the surface maximum molecular density term, allowing only the equilibrium constant  $k$  to be determined by the fitting equation. In this chapter, we primarily compare the  $k$  values for both cases. In essence, we compare the Gibbs free energy of adsorption of molecules from bulk to the air-water interface in both scenarios. Table 4.1 lists the fitting parameters for the two curves. Our experiments revealed a tenfold increase in the equilibrium constant ( $k$ ) in aerosol scenarios compared to flat surfaces, accompanied by a 1.5 kcal/mol increase in Gibbs free energy. This suggests that organic dye molecules migrate toward the aerosol surface significantly faster, indicating a fundamental difference in molecule behavior at aerosol surfaces with potentially far-reaching implications for understanding atmospheric chemical processes.

A central hypothesis emerging from our study is the influence of temperature variations in aerosols. We refer to the Gibbs free energy equation ( $\Delta G = \Delta H - T\Delta S$ ) to support this hypothesis. The migration of dye molecules from the bulk to the surface, associated with a negative entropy change ( $\Delta S$ ), means that a decrease in temperature leads to an increase in Gibbs free energy, thus favoring the migration process. In the bulk solution, these molecules are randomly oriented, contributing to higher entropy. However, at the surface, they adopt a more organized structure, leading to lower entropy. This structural reorganization at the interface is fundamental for generating strong second-order nonlinear signals at the interface, as observed through SHG. Consequently, a negative entropy change ( $\Delta S$ ) diminishes when molecules move from bulk to the air-water interface.<sup>(7)</sup> However, quantifying temperature decay is challenging. Intuitively, the transportation of aerosols in carrier gas, coupled with water evaporation and the low temperature of the carrier gas, could lower the aerosol temperature. A decreased temperature, along with a negative entropy change, would result in a more negative Gibbs free energy, corresponding to a larger  $k$  value. Further work is needed to quantitatively explain this phenomenon observed in our experiments.

Another factor potentially contributing to the difference between curved aerosol droplet surfaces and flat air-water interfaces is surface tension. Literature indicates that only when the radius of droplets is smaller than  $10^{-6}$  cm is there a detectable decrease in surface tension, which is not applicable to our case with aerosol radius over 100 nm.<sup>(8,9)</sup> However, even with comparable surface tensions, the pressure beneath the surface

differs. The Young-Laplace equation describes this pressure difference, indicating that pressure from the bulk to the surface increases as the radius decreases.*(10,11)*

$$\Delta P = \frac{2\gamma}{r} \quad (8)$$

where  $\gamma$  is the surface tension and  $r$  represent the radius of the droplet. For a 100 nm aerosol droplet, the Laplace pressure beneath the surface can reach 14 atm. This significant internal pressure may accelerate the migration process of water-soluble organic molecules in aerosols. Further experiments are necessary to confirm this hypothesis.

Additionally, our findings align with other researchers' observations of accelerated chemical reactions in microdroplets. Dr. Richard Zare and other researchers found that reactions in the microdroplet phase are faster than in the solution phase, potentially due to differences in surface pH and polarity at the microdroplet surface.*(12–15)* This phenomenon suggests a broader pattern where microdroplets, similar to aerosols, act as catalysts, speeding up reactions that would otherwise proceed more slowly on flat surfaces.

It is also worth comparing the surface molecular densities in these two scenarios. From the fitting equation, we cannot directly determine the maximum surface molecular density. However, literature suggests that at a fully Langmuir-covered flat air-water interface, the distance between organic molecules is about 2 nm,*(16,17)* with a number density of molecules in the order of  $10^{13}$ . In contrast, our fitting results, as shown in Table 2.1, indicate that the surface maximum molecular density for aerosols is in the order of  $10^9$ . This discrepancy highlights a significant difference between the two air-water interfaces. In the aerosol scenario, figure 4.3(a), the supply of molecules within

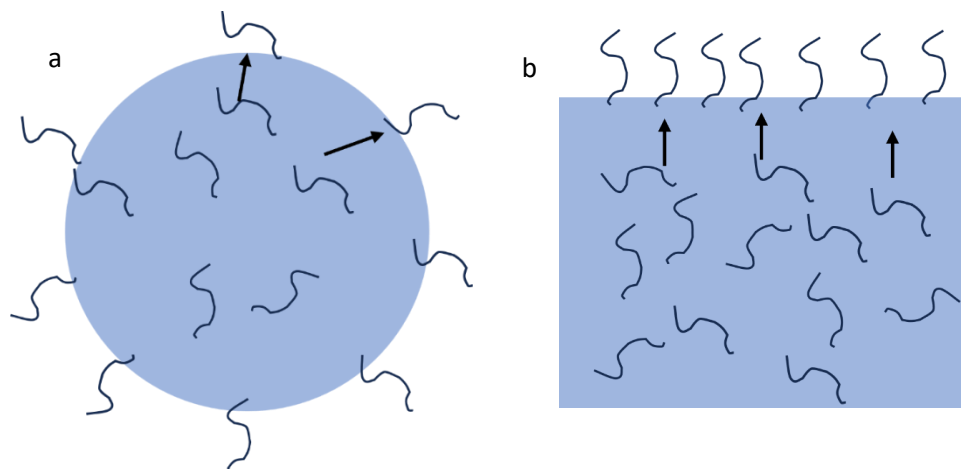


**Figure 4.3** Depiction of the equilibrium between bulk and surface in (a) aerosol and (b) flat air-water interface.

each droplet is limited. However, in the flat surface scenario, figure 4.3(b), the supply of molecules in the bulk is essentially unlimited. When a molecule migrates to the flat air-water interface, the depletion of molecules in the bulk is negligible. This observation underscores the importance of using a modified Langmuir fitting model in aerosol studies and highlights that aerosol surface properties differ from those of a flat air-water interface for several reasons. Understanding the aerosol air-water interface is crucial for better comprehension of molecule partitioning at aerosol surfaces and the associated environmental concerns.

#### 4.4 Conclusion

In this chapter, we delve into the study of organic dye molecules' dynamic equilibrium at aerosol surfaces, contrasting it with their behavior at flat air-water interfaces. Using both the Langmuir adsorption model and a modified version for aerosols, the key finding is the tenfold increase in the equilibrium constant ( $k$ ) and an increase in Gibbs free energy in aerosol scenarios compared to flat surfaces, indicating a significantly faster migration of organic molecules towards aerosol surfaces. This phenomenon is hypothesized to be influenced by temperature decrease within aerosols, driven by factors such as the temperature of the carrier gas and water evaporation, as well as the negative sign of entropy change during the process. Another possibility is the high Laplace pressure inside the droplet could accelerate the equilibrium process.

The chapter further aligns with other research findings that have observed accelerated chemical reactions in microdroplets, suggesting a broader principle where microenvironments at aerosol surfaces catalyze faster reactions. This insight is pivotal in atmospheric chemistry, highlighting the unique behavior of molecules in aerosol microenvironments. Additionally, a comparative analysis of surface molecular densities between aerosol and flat air-water interfaces reveals substantial differences, primarily due to the limited supply of molecules in aerosol droplets versus the nearly unlimited supply in bulk solutions. This finding underscores the necessity of employing a modified Langmuir model for aerosol studies and points to the distinct and influential properties of aerosol surfaces. The chapter concludes by underscoring the importance of these findings

in enhancing our understanding of atmospheric processes and their implications for environmental science, calling for further research in this vital area.

#### 4.5 Bibliography

1. Shen, Y. Optical Second Harmonic Generation At Interfaces. *Annual Review of Physical Chemistry* **1989**, 40(1), 327–350. doi:10.1146/annurev.physchem.40.1.327.
2. Jho, C.; Nealon, D.; Shogbola, S.; King, A. D. Effect of pressure on the surface tension of water: Adsorption of hydrocarbon gases and carbon dioxide on water at temperatures between 0 and 50°C. *Journal of Colloid And Interface Science* **1978**, 65(1), 141–154. doi:10.1016/0021-9797(78)90266-7.
3. Devlin, S. W.; Benjamin, I.; Saykally, R. J. On the mechanisms of ion adsorption to aqueous interfaces: air-water vs. oil-water. *Proceedings of the National Academy of Sciences of the United States of America* **2022**, 119(42), 1–7. doi:10.1073/pnas.2210857119.
4. Ruiz-Lopez, M. F.; Francisco, J. S.; Martins-Costa, M. T. C.; Anglada, J. M. Molecular reactions at aqueous interfaces. *Nature Reviews Chemistry* **2020**, 4(9), 459–475. doi:10.1038/s41570-020-0203-2.
5. Ruehl, C. R.; Davies, J. F.; Wilson, K. R. Droplet Formation on Organic Aerosols. *Science* **2016**, 351(6280), 1447–1450. doi:10.1126/science.aad4889.
6. Koenig, F. O. On the thermodynamic relation between surface tension and curvature. *The Journal of Chemical Physics* **1950**, 18(4), 449–459. doi:10.1063/1.1747660.
7. Valsaraj, K. T. Hydrophobic compounds in the environment: Adsorption equilibrium at the air-water interface. *Water Research* **1994**, 28(4), 819–830. doi:10.1016/0043-1354(94)90088-4.
8. Tolman, R. C. The effect of droplet size on surface tension. *The Journal of Chemical Physics* **1949**, 17(3), 333–337. doi:10.1063/1.1747247.

9. Ahn, W. S.; Jhon, M. S.; Pak, H.; Chang, S. Surface tension of curved surfaces. *Journal of Colloid And Interface Science* **1972**, *38*(3), 605–608. doi:10.1016/0021-9797(72)90395-5.
10. Malek, S. M. A.; Poole, P. H.; Saika-Voivod, I. Thermodynamic and structural anomalies of water nanodroplets. *Nature Communications* **2018**, *9*(1). doi:10.1038/s41467-018-04816-2.
11. Malek, S. M. A.; Sciortino, F.; Poole, P. H.; Saika-Voivod, I. Evaluating the Laplace pressure of water nanodroplets from simulations. *Journal of Physics Condensed Matter* **2018**, *30*(14). doi:10.1088/1361-648X/aab196.
12. Banerjee, S.; Gnanamani, E.; Yan, X.; Zare, R. N. Can all bulk-phase reactions be accelerated in microdroplets? *Analyst* **2017**, *142*(9), 1399–1402. doi:10.1039/c6an02225a.
13. Tuck, A. F. Gibbs free energy and reaction rate acceleration in and on microdroplets. *Entropy* **2019**, *21*(11). doi:10.3390/e21111044.
14. Xiong, H.; Lee, J. K.; Zare, R. N.; Min, W. Strong Electric Field Observed at the Interface of Aqueous Microdroplets. *Journal of Physical Chemistry Letters* **2020**, *11*(17), 7423–7428. doi:10.1021/acs.jpcelett.0c02061.
15. Lee, J. K.; Samanta, D.; Nam, H. G.; Zare, R. N. Micrometer-Sized Water Droplets Induce Spontaneous Reduction. *Journal of the American Chemical Society* **2019**, *141*(27), 10585–10589. doi:10.1021/jacs.9b03227.
16. Wang, H.; Troxler, T.; Yeh, A. G.; Dai, H. L. In situ, nonlinear optical probe of surfactant adsorption on the surface of microparticles in colloids. *Langmuir* **2000**, *16*(6), 2475–2481. doi:10.1021/la9909087.
17. Xu, B.; Gonella, G.; Delacy, B. G.; Dai, H. L. Adsorption of anionic thiols on silver nanoparticles. *Journal of Physical Chemistry C* **2015**, *119*(10), 5454–5461. doi:10.1021/jp511997w.

## CHAPTER 5 CONCLUSION AND PROSPECTIVES

This dissertation has successfully explored the intricate behaviors of water-soluble organic molecules on atmospheric aerosol surfaces through the innovative use of Second Harmonic Scattering (SHS). The study's primary focus on the partitioning of these molecules at the aerosol surface has not only enriched our understanding of atmospheric chemistry but also highlighted the crucial role aerosols play in processes affecting cloud formation, radiation balance, and air quality.

In the first segment of the research, the disposition of organic molecules on aerosol surfaces was examined. The use of a modified Langmuir model to describe this behavior underscored the predominance of these molecules on the aerosol surface, thus emphasizing the surface's significant role in atmospheric reactions.

The second segment delved into the interactions between salts and organic molecules on the aerosol surface. The varying influences of different ions on the partitioning behavior of organic molecules were revealed, illustrating the vital importance of ionic species in governing aerosol surface dynamics.

The final segment of the study brought to light a notable difference between aerosol and planar air-water interfaces. The discovery of a tenfold faster equilibrium rate constant for aerosols, indicative of a larger Gibbs free energy, sets apart the unique kinetic and thermodynamic behaviors of aerosol surfaces from their planar counterparts.

This finding is pivotal in understanding the lesser molecular density on aerosol surfaces due to the finite availability of organic molecules.

Overall, this dissertation marks a significant advancement in aerosol science. The introduction of a novel in-situ technique for detecting organic molecules at aerosol surfaces represents a breakthrough in the field, offering profound insights into the distribution and interactions of these molecules within atmospheric particles.

Looking ahead, the prospects for further research in this area are vast. Future studies could explore the implications of these findings on the global climate model, particularly in understanding aerosol-cloud interactions and their effects on weather patterns and climate change. Additionally, the impact of varying atmospheric conditions on aerosol surface chemistry warrants deeper investigation. The potential health impacts of aerosols, given their pervasive nature and interaction with environmental pollutants, also present a significant area for future research. Lastly, the refinement and application of SHS in other atmospheric contexts could provide even greater insights into the complex world of atmospheric sciences.

In conclusion, the insights gained from this study have crucial implications for our comprehensive understanding of climate change, air quality, and the environmental and health impacts of aerosols, underlining the need for continued exploration in this field.